THEORETICAL INVESTIGATIONS OF H(D) + HBr(DBr) ABSTRACTION AND EXCHANGE REACTIONS

By

MEENAKSHISUNDARAM PADMASANI SUDHAKARAN

Bachelor of Science
University of Madras
Madras, India
1979

Master of Science
University of Madras
Madras, India
1981

Submitted to the Faculty of the Graduate College
of the Oklahoma State University
in partial fulfillment of the requirements
for the Degree of
MASTER OF SCIENCE
May, 1985

THEORETICAL INVESTIGATIONS OF H(D) + HBr(DBr)

ABSTRACTION AND EXCHANGE REACTIONS

Thesis Approved:

Lionel M. Raff
Thesis Adviser

K D Berlin

Donald L. Thompson

Norman N Durham
Dean of the Graduate College

ACKNOWLEDGMENTS

It is with a profound sense of indebtedness that I wish to place on record my sincere thanks to Dr. Lionel M. Raff for having suggested the problem and for his constant guidance, advice, suggestions and encouragement during the course of the work and during the preparation of this thesis.

I gratefully acknowledge Dr. D. L. Thompson and Dr. K. D. Berlin for their help and advice as members of my advisory committee.

I would also like to thank Dr. Neil Purdie, Chairman of the Department of Chemistry for having provided me with the necessary facilities. Help from various individuals of the OSU computer center, too numerous to identify, is also kindly acknowledged.

I have great pleasure in expressing my very sincere thanks to Dr. I. NoorBatcha for his useful suggestions and advice at various stages of this investigation.

I am completely indebted to Dr. (Mrs.) Ponnammal Natarajan and Dr. K. R. Natarajan in many different ways for their continuous encouragement and assistance during my entire career.

I thank Ms. Sue Heil for typing the final copy of this thesis in an excellent manner within a short interval of time.

Writing a thesis like this is never a private project. Hence, acknowledgment is also made of the helpful discussions with fellow graduate students of this group and of the Department of Chemistry of OSU.

To my family.

TABLE OF CONTENTS

LIST OF TABLES

LIST OF FIGURES

CHAPTER I

INTRODUCTION

Elementary reactions involving transfer of a hydrogen atom or a halogen atom have had a major role in the development of chemical kinetics. Theoretical studies of D + HX and H + DX (X = Cl, Br or I) systems include construction of semiempirical, potential-energy surfaces (1), statistical phase-space treatments of the abstraction to exchange ratio (2, 3) and quasiclassical trajectory calculations. Many experimental and theoretical investigations have been made to determine the energy barrier for both abstraction and exchange processes of H + DX system of reactions. The following notation will be used throughout this thesis:

$$H(D) + HX(DX) \text{ - - - } \rightarrow H_2\ (HD,\ D_2) + HBr(DBr)$$

(abstraction) (R1)

$$H(D) + H'X(D'X) \text{ - - - } \rightarrow HX(DX) + H'(D')$$

(exchange) (R2)

where X is a halogen atom. For simplicity, the reaction H + DBr will be denoted by (H, D) with similar notation for the other isotopic combinations.

Several molecular beam studies of the D + HX exchange and abstraction reactions have also been carried out (4, 5, 6). Persky and Kuppermann (7) have photolytically measured the abstraction fraction in the reaction of a deuterium atom with HX where X = Br or I.

Reactions of atomic hydrogen and deuterium with HBr and DBr have recently been studied by Endo and Glass (8) over the temperature range of 230-318 K using a discharge flow apparatus equipped for EPR detection of atoms. From their experimental work, these authors have concluded that potential-energy barriers of approximately 2 kcal/mole and 5 kcal/mole must be present for linear H-H-Br and H-Br-H configurations, respectively. Similar results at 300 K have been obtained by Husain and Slater (9). Botschwina and Meyer (10) have estimated that the barrier height for the exchange reaction of H' + BrH ⟶ H'Br + H lies in the region of 3-11 kcal/mole.

A review of studies on potential-energy surfaces for atom transfer reactions involving hydrogens and halogens has been published by Parr and Truhlar (11). In a very recent theoretical work on H + HX, where X = F-I, Dunning (12) has predicted higher barriers for the exchange reactions than for the corresponding abstraction processes. However, he points out that his calculations, generalized valence bond CI, are not the most accurate type available (or possible) for these systems although they are of uniformly high quality.

In 1981, Hepburn, Klimek, Liu, Macdonald, Northrup and Polanyi (13) studied the abstraction reaction

$$H(D) + HBr(DBr) \dashrightarrow H_2\ (HD,\ D_2) + Br$$

using a crossed molecular beam experiment and have reported relative cross sections as a function of collision energy. They employed a supersonic source for the input of H or D atoms and used a tunable vacuum UV laser to obtain laser-induced fluorescence of •Br. These workers concluded that a negligible barrier (< 1 kcal/mole) must exist for the HHBr configuration while a barrier of about 5 kcal/mole is

anticipated for the HBrH linear geometry. Furthermore, molecular beam measurements of the total D + HBr scattering cross section by Toennies and coworkers (14) indicate that the potential-energy surface contains no attractive wells deeper than 9.06 meV (0.209 kcal/mole).

Several classical trajectory studies on various isotopic combinations of Reactions (R1) and (R2) have been reported. Parr and Kuppermann (PK) (15) computed reaction cross sections for the H + DBr abstraction reaction on a surface which had a 1.75 kcal/mole barrier for H···H···Br abstraction and a 3.96 kcal/mole barrier for exchange with no attractive wells. The computed reaction cross sections exhibited a clear threshold near 1.0 kcal/mole due to the presence of the abstraction barrier. In contrast, the molecular beam data (13) show no such threshold. A second study by White and coworkers (16) employed a modified LEPS surface with no barrier to abstraction, a 1.0 kcal/mole barrier to exchange, and three potential wells about 2-3 kcal/mole in depth. Abstraction cross sections computed on this surface show no threshold behavior but the amount of exchange observed was too large due to the low barrier.

Trajectory calculations have also been reported by Hepburn and coworkers as part of the analysis of their molecular beam data (13). Collinear calculations on the PK surface showed a sequence of abstraction cross sections (D,D) > (H,D) > (H,H) > (D,H) at a collision energy of 7.0 kcal/mole whereas the molecular beam data gave (D,H) > (D,D) > (H,H) > (H,D) at this collision energy. Three-dimensional calculations on the same potential energy surface were in better accord with experiment, but the ordering of the (H,H) and (D,D) reactions was inverted.

There is now sufficient information concerning the topography of the (H_2Br) potential surface and sufficient experimental data that one might expect to obtain accurate dynamical information for Reactions (R1) and (R2) with X = Br from classical trajectory calculations. By adjustment of the surface to fit the calculated reaction cross sections and rates to the experimental data as closely as possible, an even more accurate estimate of the abstraction barrier might be obtained.

In this present work, we report the results of such calculations. Three London-Eyring-Polanyi-Sato (LEPS) surfaces have been used to investigate the reaction dynamics of R1 and R2 for X = Br. The abstraction barriers range from 0.19 to 1.01 kcal/mole while the barrier for exchange is about 5 kcal/mole. There are no attractive wells present whose depth exceeds 9.08 meV. The computed relative cross sections on each surface are compared with the results of Hepburn and coworkers (13) in an effort to determine the abstraction barrier more precisely. In addition, rate calculations at two different temperatures have also been carried out to determine activation energies. These results are compared to the thermal data reported by Endo and Glass (8) and by Husain and Slater (9). In addition, we also computed differential scattering cross section and product energy distributions for all isotopic combinations of Reactions (R1) and (R2) for X = Br.

The method employed in this theoretical investigation along with the results obtained and the model developed to interpret them are described in the following sections.

CHAPTER II

COMPUTATIONAL METHODS

A. Potential-Energy Surfaces

The first phase in the study of collision dynamics is the determination of the potential energy of the system being studied, i.e., finding the interaction energy of the particles which comprise the system as a function of their relative positions. The representation of the potential energy of a system involving more than two atoms is generally termed the potential-energy surface. The topographical details of such a hypersurface can be conveniently represented in the form of a map showing energy contours as a function of suitable bond distances and angles.

In this present calculation, the London-Eyring-Polanyi-Sato (LEPS) formalism has been used (17). The parameterized form of the LEPS surface used is

$$V(r_1,r_2,r_3) = (Q_1/(1+a)) + (Q_2/(1+b)) + (Q_3/(1+c)) - \Big[J_1^2/(1+a)^2 + J_2^2/(1+b)^2 + J_3^2/(1+c)^2 - J_1J_2/(1+a)(1+b) - J_2J_3/(1+b)(1+c) - J_1J_3/(1+a)(1+c) \Big]^{\frac{1}{2}} \quad (1)$$

where

$$Q_1/(1+a) = (1/2)\left[{}^1E(r_1) + ((1-a)/(1+a))\ {}^3E(r_1) \right] \quad \text{and} \quad (2)$$

$$J_1/(1+a) = (1/2)\left[{}^1E(r_1) - ((1-a)/(1+a))\ {}^3E(r_1)\right] \qquad (3)$$

with similar expressions for $Q_2(Q_3)$ and $J_2(J_3)$ where 'a' is replaced by 'b' or 'c' and r_1 by r_2 or r_3. Morse and 'anti-Morse' type functions have been used to represent the singlet and triplet energy states of the molecule, respectively:

$${}^1E(r) = D(\exp(-2\alpha(r-r_e))-2\exp(-\alpha(r-r_e))) \qquad (4)$$

and

$${}^3E(r) = (1/2)D(\exp(-2\alpha(r-r_e))+2\exp(-\alpha(r-r_e))) \qquad (5)$$

values of D, and R are evaluated as follows:

D = experimental dissociation energy + zero-point energy of the diatomic molecule,

r_e = equilibrium separation of diatomic molecule, and

$$\alpha = \Pi\nu_0(2\mu/D)^{\frac{1}{2}} \qquad (6)$$

where μ is the reduced mass of the diatomic i-j system. It can also be noted that α represents the requirement that the curvature of ${}^1E_{ij}$ near r_e be such that the experimental value for the fundamental vibration frequency ν_o is reproduced accurately.

In these expressions, for a general reaction of the type A + BC - - - → AB + C, r_1, r_2 and r_3 denote the distances between AB, BC and CA, respectively. Clearly, for a linear case, $r_3 = r_1 + r_2$. The quantities a, b and c are the Sato parameters. The various parameter values that have been used in constructing the LEPS surfaces are shown in Table I, and the molecular units employed are the same as listed in reference (20).

The experimental results of Hepburn and coworkers (13) and Toennies

TABLE I

MORSE PARAMETERS FOR THE H_2 AND HBr SINGLET AND TRIPLET-STATE FUNCTIONS

Molecule	Parameter			Reference
	D(eV)	$\alpha(a\cdot u)^{-1}$	$r_e(a\cdot u)$	
H_2	4.7466	1.027	1.402	18
HBr	3.918	0.9588	2.673	19

and coworkers (14) indicate that the potential-energy surface with X = Br should have the following features:

a. An abstraction reaction barrier less than 1 kcal/mole;

b. An exchange reaction barrier of about 5 kcal/mole; and

c. No attractive wells whose depth is greater than 0.209 kcal/mole.

Since the barrier height, E_b, corresponds to the energy at the saddle point, a brief description of the methods utilized to locate the saddle point now follows.

Let us suppose that a function f and its partial derivatives up to and including those of the third order are continuous near the point (μ, v) and further that $f_x(\mu, v) = f_y(\mu, v) = 0$. For such a condition, we have a saddle point if (21)

$$f_{xx}(\mu,v)\, f_{yy}(\mu,v) - f^2_{xy}(\mu,v) < 0, \tag{7}$$

where

$$f_x = \partial f/\partial x,$$

and

$$f^2_{xy} = \partial^2 f/\partial y \partial x, \tag{8}$$

with analogous definitions for f_{xx} and f_{yy}.

In the present problem, the potential-energy function V has three variables, r_1, r_2, r_3. Thus, the problem of finding the saddle point reduces to finding a set of r_1 and r_2 (r_3) values for a given set (a,b,c) of Sato parameters such that the surface meets all expected features described above.

In the numerical determination of the saddle point, a search has been made with equal values of r_1 and r_2 for the exchange process

because of the involved symmetry. For the abstraction process, the value of r_1 is fixed while the value of r_2 is varied and the corresponding potential-energy values calculated. This process is repeated with various fixed values of r_1. Finally, the computed values are printed as a square matrix with ten rows and columns. For any particular column or row, the potential-energy values may either decrease or increase monotonically if it is not near the saddle point. However, near the saddle point the potential-energy values will decrease from top to bottom in a column, reach a minimum, and then increase. At the same time, across a row the potential-energy values will increase, attain a maximum, and then decrease. The crossing of these two trends locates the saddle point for an abstraction reaction.

In the case of an exchange process, $\partial V/\partial r_1$, $\partial V/\partial r_2$, $\partial^2 V/\partial r_1^2$, $\partial^2 V/\partial r_2^2$ and $\partial^2 V/\partial r_2 \partial r_1$ are first evaluated. Whenever $\partial V/\partial r_1 = \partial V/\partial r_2 = 0$,

$$\left(\frac{\partial^2 V}{\partial r_1^2}\right)\left(\frac{\partial^2 V}{\partial r_2^2}\right) - \left[\frac{\partial^2 V}{\partial r_2 \partial r_1}\right]^2$$

is computed. If this quantity is less than zero, a saddle point has been obtained. Actually, there exists a practical difficulty in obtaining an exact zero on the computer. In order to overcome this, a parameter 'epsilon' is defined in the code and is adjusted to its minimum.

Thus, with different sets of Sato parameters, the corresponding saddle points have been determined. The characteristics of all three surfaces employed in this work are listed in Table II. Representative contour maps of a few surfaces are also shown in Figures 1 through 8. In all cases, the lowest value for E_b is observed for the linear system

TABLE II

SURFACE CHARACTERISTICS: SADDLE-POINT POSITION AND BARRIER HEIGHTS

Surface	A-B-C Angle (degrees)	Abstraction		Exchange	
		(R_1,R_2) a·u	E_b (eV)	(R_1,R_2) a·u	E_b (eV)
I	180	2·1, 2·8	0.04386	3·0, 3·0	0.2253
	135	2·0, 2·9	0.2154	3·0, 3·0	0.2403
	90	2·0, 3·2	1.201	3·0, 3·0	0.3541
II	180	2·1, 2·8	0.02833	3·0, 3·0	0.2094
	135	2·0, 2·9	0.1974	3·0, 3·0	0.2241
	90	2·0, 3·2	1.178	3·0, 3·0	0.3373
III	180	2·2, 2·8	0.008264	3·0, 3·0	0.2242
	135	2·0, 2·9	0.1818	3·0, 3·0	0.2386
	90	2·0, 3·2	1.175	3·0, 3·0	0.3478

Sato parameters: Surface I: (0.26, 0.06, 0.06)

Surface II: (0.265, 0.0645, 0.0645)

Surface III: (0.28, 0.06, 0.06)

Figure 1. Contour Map for Collinear $H\underset{R_1}{\text{—}}H\underset{R_2}{\text{—}}Br$, $\theta = 180^{o}$ on Surface I.

Contour values are given in eV on this contour map.

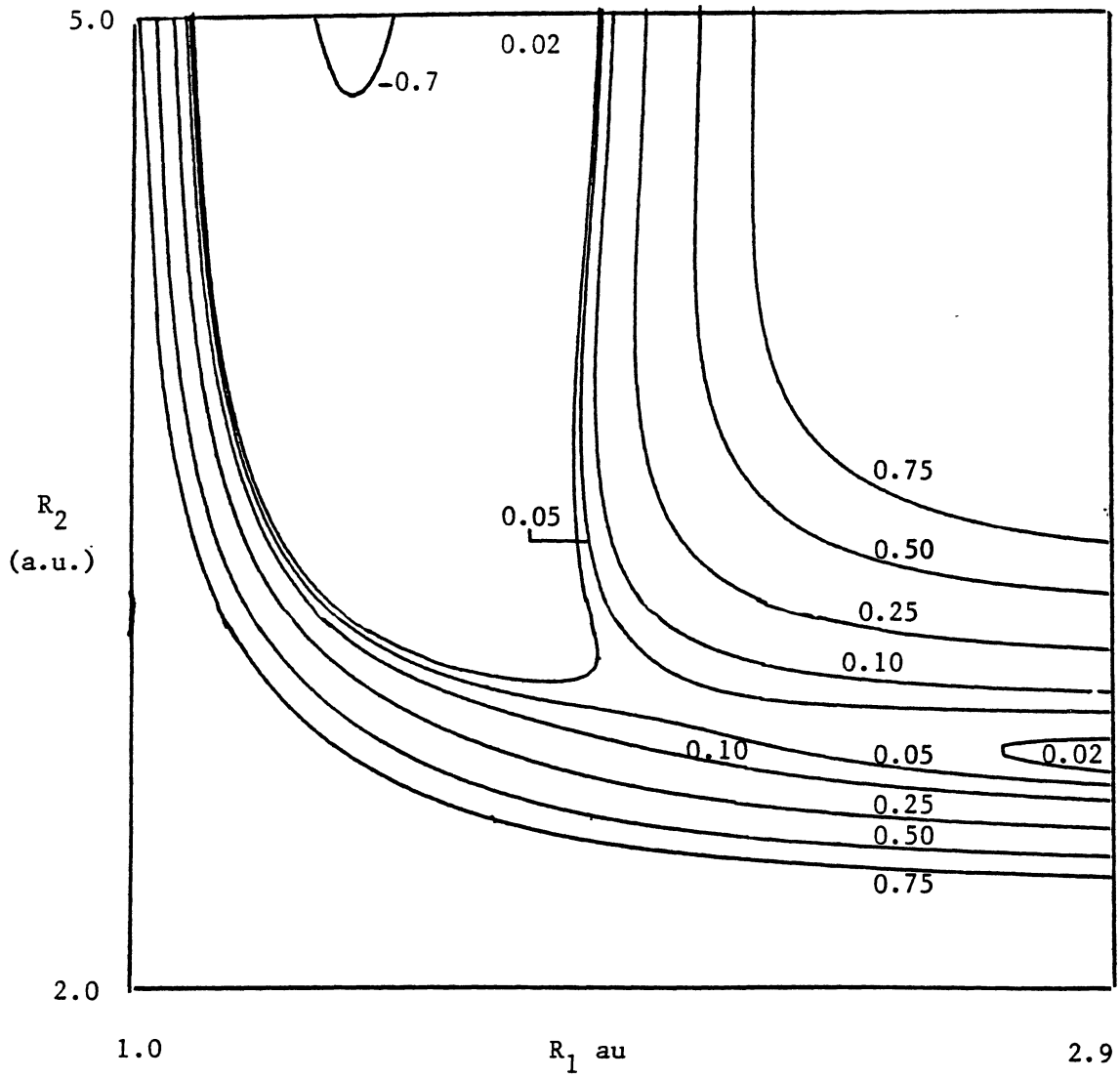
5.0
2.0
1.0
2.9
R_2
(a.u.)
R_1 au
-0.7
0.02
0.05
0.10
0.25
0.50
0.75
0.10
0.05
0.02
0.25
0.50
0.75

Figure 2. Contour Map for Collinear $H\underset{R_1}{\text{—}}H\underset{R_2}{\text{—}}Br$, $\theta = 135^{o}$ on Surface I. Contour values are given in eV on this contour map.

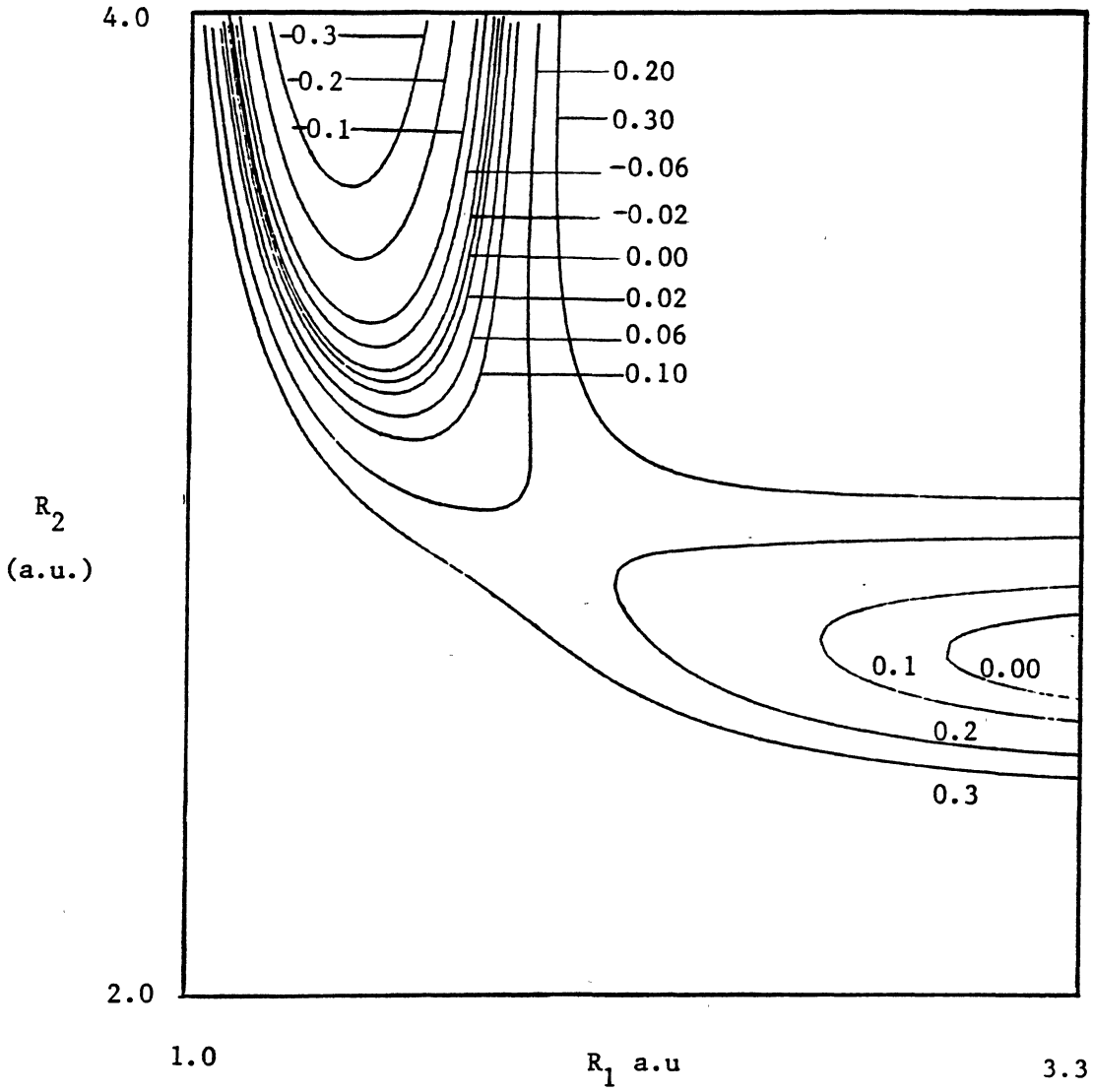
4.0
2.0
1.0
3.3
R_2
(a.u.)
R_1 a.u
-0.3
-0.2
-0.1
0.20
0.30
-0.06
-0.02
0.00
0.02
0.06
0.10
0.1
0.00
0.2
0.3

Figure 3. Contour Map for Collinear $H\underset{R_1}{—}H\underset{R_2}{—}Br$, $\theta = 135^{o}$ on Surface II. Contour values are given in eV on this contour map.

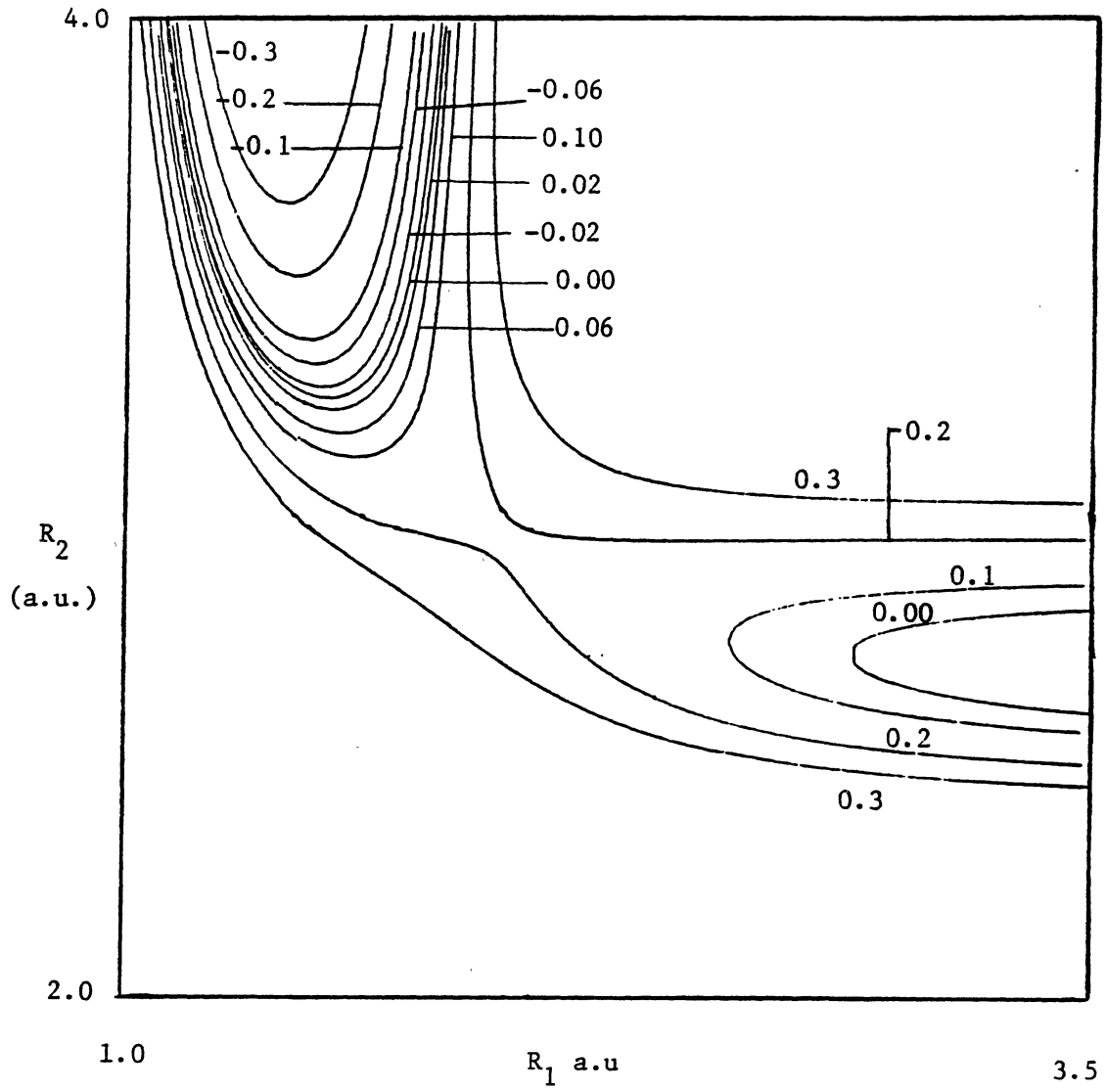
4.0
-0.3
-0.2
-0.1
-0.06
0.10
0.02
-0.02
0.00
0.06
0.2
0.3
0.1
0.00
0.2
0.3
R_2
(a.u.)
2.0
1.0
R_1 a.u
3.5

Figure 4. Contour Map for Collinear $H\underset{R_1}{\text{—}}Br\underset{R_2}{\text{—}}H$, $\theta = 180^{o}$ on Surface II. Contour values are given in eV on this contour map.

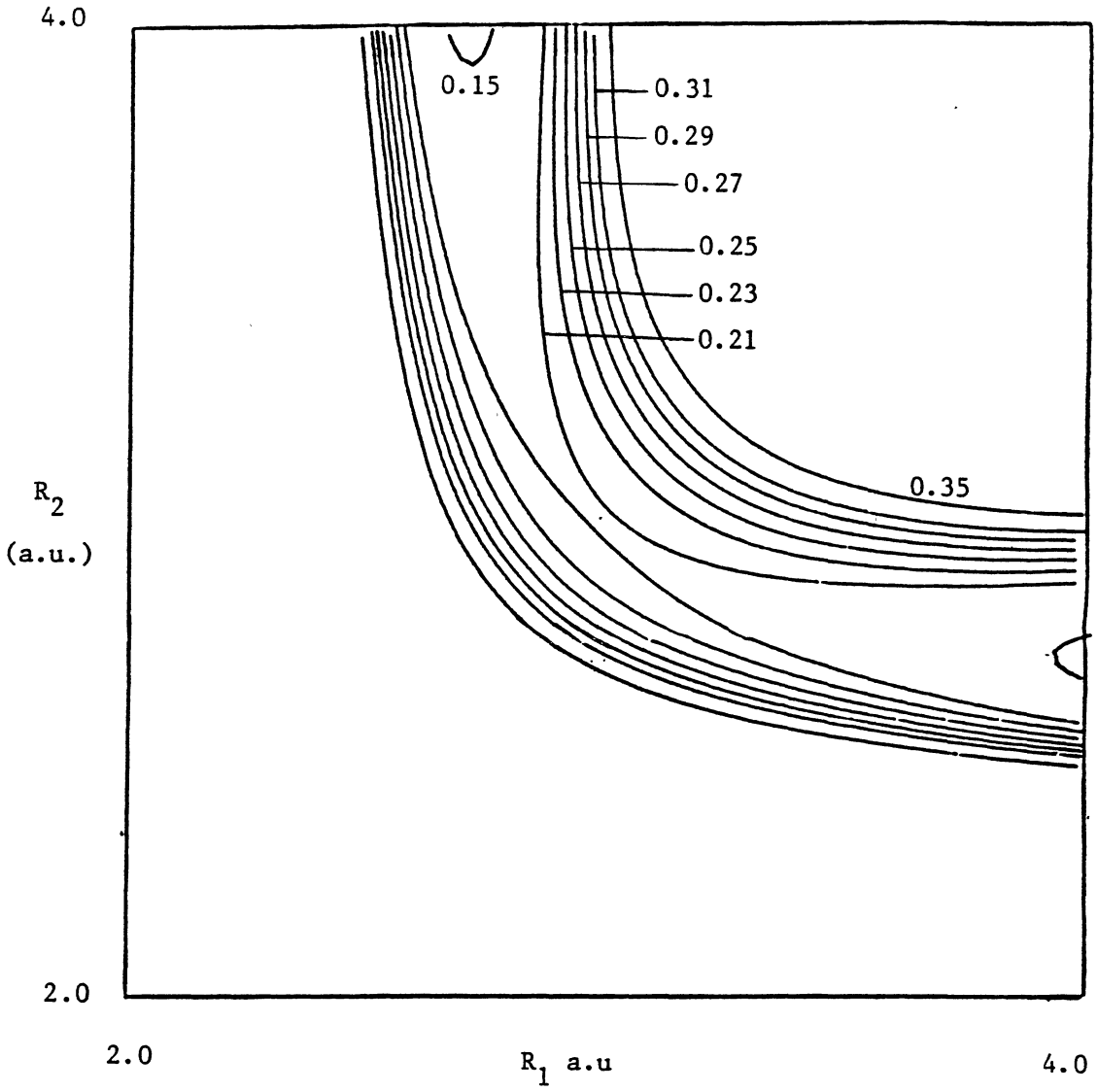
4.0
0.15
0.31
0.29
0.27
0.25
0.23
0.21
0.35
R_2
(a.u.)
2.0
2.0
R_1 a.u
4.0

Figure 5. Contour Map for Collinear $H\underset{R_1}{—}Br\underset{R_2}{—}H$, $\theta = 90^{o}$ on Surface III. Contour values are given in eV on this contour map.

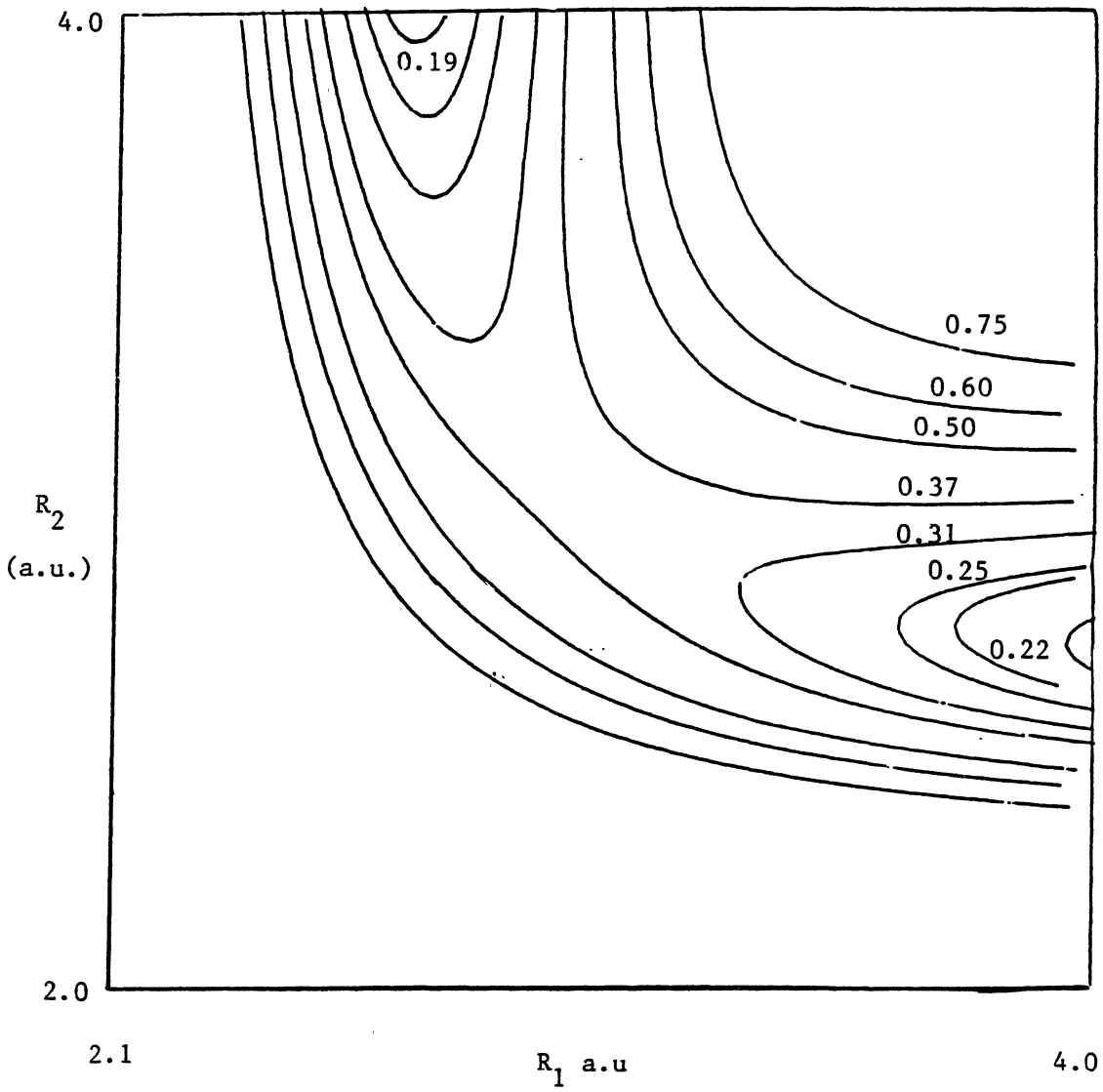
4.0
0.19
0.75
0.60
0.50
0.37
0.31
0.25
0.22
R_2
(a.u.)
2.0
2.1
R_1 a.u
4.0

Figure 6. Contour Map for Collinear $H\underset{R_1}{\text{—}}Br\underset{R_2}{\text{—}}H$, $\theta = 135^{o}$ on Surface III.

Contour values are given in eV on this contour map.

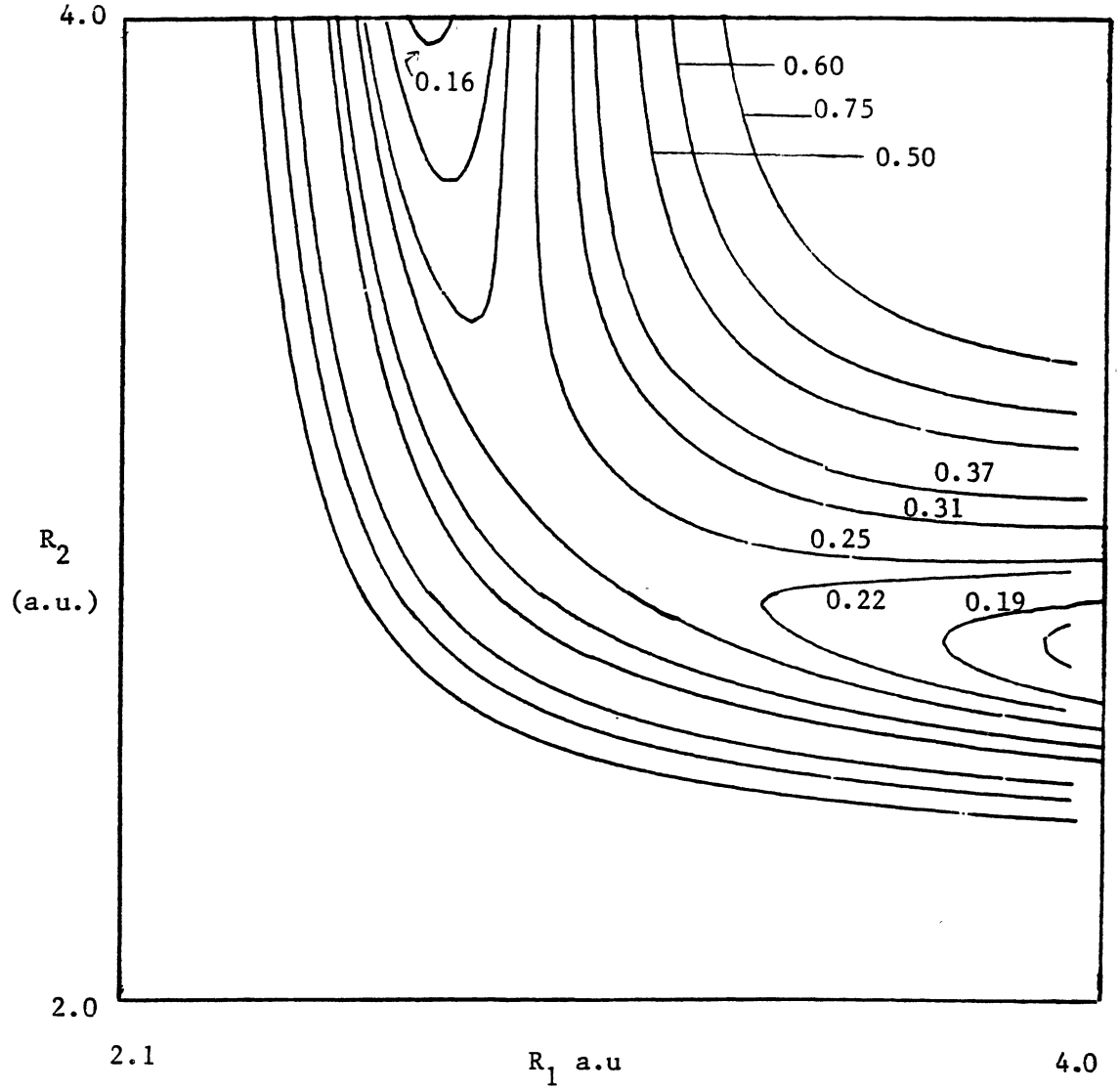
4.0
0.16
0.60
0.75
0.50
0.37
0.31
0.25
0.22
0.19
R_2
(a.u.)
2.0
2.1
R_1 a.u
4.0

Figure 7. Contour Map for Collinear $H\underset{R_1}{—}Br\underset{R_2}{—}H$, $\theta = 180^{o}$ on Surface III. Contour values are given in eV on this contour map.

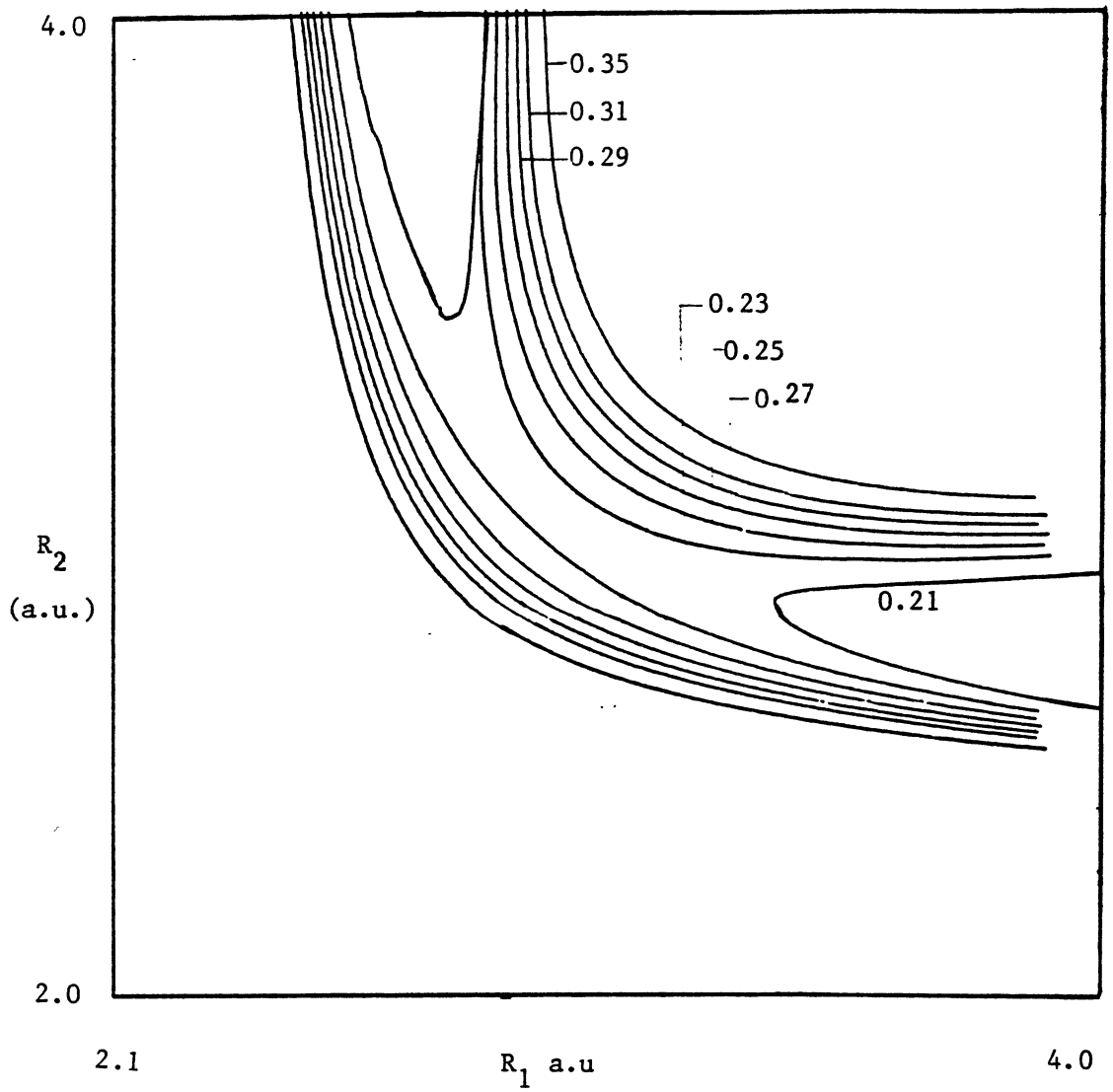
4.0
2.0
2.1
4.0
R_1 a.u
R_2
(a.u.)
-0.35
-0.31
-0.29
-0.23
-0.25
-0.27
0.21

Figure 8. Contour Map for Collinear $H\underset{R_1}{\text{—}}Br\underset{R_2}{\text{—}}H$, $\theta = 180^{o}$ on Surface I.

Contour values are given in eV on this contour map.

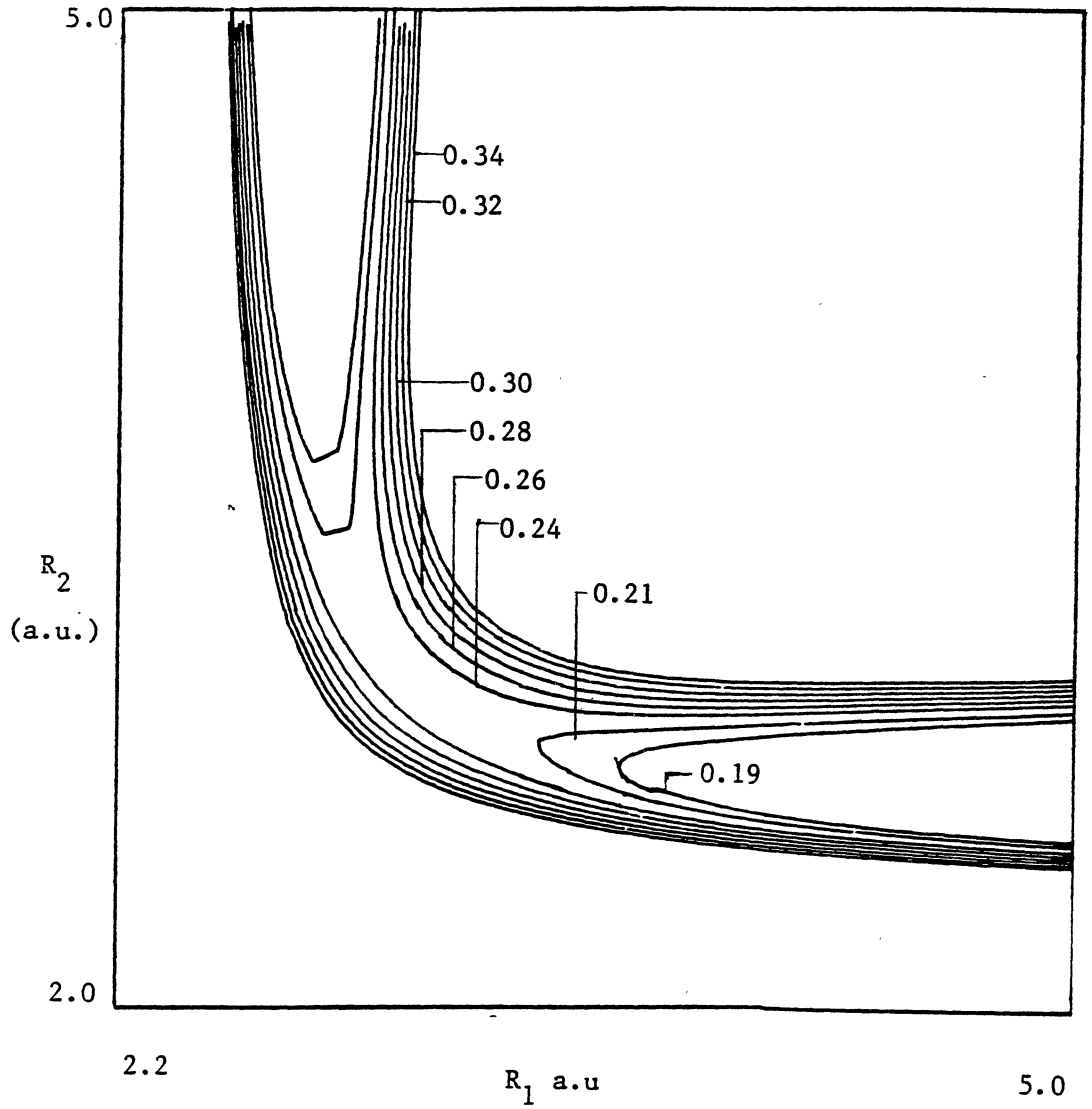
5.0
0.34
0.32
0.30
0.28
0.26
0.24
0.21
0.19
R_2
(a.u.)
2.0
2.2
R_1 a.u
5.0

with $\theta = 180^{\circ}$. This is what one would expect for three-body systems involving primarily s-orbital type bonding. It should be noted that for all surfaces the lowest exchange reaction barrier lies in the range 4.83 to 5.20 kcal/mole while the lowest abstraction barriers are always 1.01 kcal/mole or less. Furthermore, a careful search of the surfaces shows that there are no attractive wells present whose depth exceeds 0.2224 kcal/mole. Therefore, surfaces I, II and III all contain the topographical features suggested by the molecular beam data (13, 14).

B. Trajectory Calculations

Having selected a surface, the next step is to compute trajectories on the same. The methods required to execute such calculations and to compute rates and cross sections from the results have been previously described by several authors (22, 23, 24). In this section we describe only those methods which deviate significantly from the standard procedures.

In the molecular beam experiments (13), the relative velocity, V_r, is fixed for the system under consideration since in Hepburn's experiment (13) all reactions have been measured at a well-defined collision energy, E_T. The initial vibrational and rotational states of the HBr (DBr) molecule, however, are selected from a Boltzmann distribution at 300 K. The initial translational and internal-states in the trajectory calculations are, therefore, selected in a corresponding manner.

The integral over the collision impact parameter, b, has the form

$$I = \int_{b=0}^{b=b_m} P(b,q)2\Pi bdb, \tag{9}$$

where P(b,q) is the reaction probability for collisions in the impact parameter range b to b+db and q represents the remaining set of variables upon which P(b,q) depends. b_m is a value such that P(b,q) = 0 for $b \geq b_m$. In order to increase the statistical accuracy of the calculations, importance sampling has been employed in the Monte Carlo evaluation of the integral in Equation 9. In this method, a selection procedure that weights the smaller impact parameters more heavily is invoked in the selection of initial conditions for the Monte Carlo evaluation of the impact parameter integral. Faist, Muckermann and Schuber (25) have given a detailed treatment of this procedure for classical trajectory applications.

Specifically, the impact parameter integral is written in the form

$$I = \int_0^{b_m} P(b,q)(P_0(b)/P_0(b))2\Pi bdb, \tag{10}$$

where $P_0(b)$ is termed the "expected distribution". We now define a new weight function

$$W(b) = N_0 P_0(b)2\Pi b, \tag{11}$$

where N is a normalization constant whose value is given by

$$N_0 = \left[\int_0^{b_m} P_0(b)2\Pi bdb\right]^{-1} \tag{12}$$

Combination of Equations 10 and 11 gives

$$I = (1/N_0)\int_0^{b_m} [P(b,q)/P_0(b)]\ W(b)db. \tag{13}$$

A second transformation can be used to put Equation 13 into a form suitable for Monte Carlo evaluation. Let

$$\xi = \int_{b=0}^{b} W(b)db, \tag{14}$$

such that

$$d\xi = W(b)db, \tag{15}$$

and hence

$$I = (1/N_0)\int_{\xi=0}^{1} [P(\xi,q)/P_0(\xi)]\ d\xi\,. \tag{16}$$

The Monte Carlo approximant for I is

$$I = \frac{1}{N_0 N}\sum_{i=1}^{N_R} [P_0(\xi_i)]^{-1} \tag{17}$$

where the ξ_i are randomly chosen from a uniform distribution on the interval (0,1). The summation is taken only over the reactive trajectories, and N is the total of trajectories computed.

In the present application, we have used two different forms for the expected distribution:

$$P_0(b) = b^{-1}, \tag{18}$$

and

$$P_0(b) = [1 - (b/b_m)^2]. \tag{19}$$

For $P_0(b) = b^{-1}$, we obtain

$$W(b) = b_m^{-1}, \tag{20}$$

and hence, from Equation 14

$$b = \xi b_m. \tag{21}$$

Equation 17 then becomes

$$I = \frac{2\Pi b_m^2}{N} \sum_{i=1}^{N_R} \xi_i. \tag{22}$$

If Equation 19 is used for the expected distribution, the results are

$$W(b) = \frac{4}{b_m^4} [b_m^2 - b^2]\, b, \tag{23}$$

$$b = b_m\, [1 - (1-\xi)^{\frac{1}{2}}]^{\frac{1}{2}}, \tag{24}$$

and

$$I = \frac{\Pi b_m^2}{2N} \sum_{i=1}^{N_R} (1-\xi_i)^{-\frac{1}{2}}. \tag{25}$$

In essence, the importance sampling weights the trajectories by ξ_i if $P_0(b) = b^{-1}$ and by $(1-\xi_i)^{-\frac{1}{2}}$ if $P_0(b) = [1-(\frac{b}{b_m})^2]$.

The initial selection of all other variables and the end tests for the final states are carried out using the usual techniques (22, 23, 24, 26). The 12 Hamiltonian equations of motion are integrated with a Runge-Kutta-Gill routine using a fixed integration step size of 0.1 t.u., where 1 t.u. = $0.53871469 \times 10^{-14}$ sec.

All multidimensional integrations are done using the Monte Carlo approximant suitably modified by the importance sampling procedures described by Equations 10-25. For such evaluation, one sigma limit of

statistical uncertainty is given by

$$\Delta = \left[\frac{N \sum_{i=1}^{N_R} (1-\xi_i)^{-1} - \left\{ \sum_{i=1}^{N_R} (1-\xi_i)^{-\frac{1}{2}} \right\}^2}{N \left\{ \sum_{i=1}^{N_R} (1-\xi_i)^{-\frac{1}{2}} \right\}^2} \right]^{\frac{1}{2}} \cdot 100 \qquad (26)$$

for the importance sampling case, $b = b_{max}[1-(1-\xi)^{\frac{1}{2}}]^{\frac{1}{2}}$, and

$$\Delta = \left[\frac{N \sum_{i=1}^{N_R} \xi_i^2 - \left[\sum_{i=1}^{N_R} \xi_i \right]^2}{N \left[\sum_{i=1}^{N_R} \xi_i \right]^2} \right]^{\frac{1}{2}} \cdot 100 \qquad (27)$$

if b is selected using Equation 21.

In the above expressions, N is the total number of trajectories employed; N_R is the number of reactive trajectories obtained and ξ_i is the random number of the i^{th} reactive trajectory.

The differential scattering cross section at angle θ_i to $(\theta_i + \Delta\theta)$ is computed from

$$I(\theta_i) = \sum_{j=1}^{N_R} P_j(\theta_i) F(\xi_i) / \text{Sin } \theta_i, \qquad (28)$$

where the sum runs over the reactive trajectories and $P_j(\theta) = 1$ if trajectory j scatters into the range θ_i to $(\theta_i + \Delta\theta)$ and zero otherwise. The weight function $F(\xi_i)$ is given by

$$F(\xi_i) = (1-\xi_i)^{-\frac{1}{2}} , \tag{29}$$

if

$$P_0(b) = 1 - \left(\frac{b}{b_m}\right)^2 \quad \text{and}$$

$$F(\xi_i) = \xi_i , \tag{30}$$

if

$$P(b) = b^{-1}.$$

Similar expressions are used to compute the internal energy distributions for the product molecules.

The internal energy distribution of the product molecules, the center-of-mass angular distributions of product atoms and the computed absolute and relative cross section values for Reactions R1 and R2 with X = Br as a function of collision energy are reported in the following chapter. In addition, calculated rate coefficient values at 250 K and 300 K are also given.

CHAPTER III

RESULTS AND DISCUSSION

The computed cross section values for the various abstraction reactions on surfaces I, II and III obtained from the results of 117,000 trajectories are presented in Tables III through VI. For the E = 7 kcal/mole case, cross section values for the exchange processes are included. Collision energies of 2 kcal/mole or less lie below the threshold for the exchange reaction. In order to compare these results with the relative cross section values reported by Hepburn and co-workers (13), the cross section values for the abstraction reactions on each surface are normalized with the $H + HBr \longrightarrow H_2 + Br$ result at E_T = 7.0 kcal/mole, as has been done in Hepburn's work (13). In all cases, the error limits represent one sigma limit of statistical uncertainty as defined by Equations 26 and 27.

The molecular beam data for the relative abstraction cross sections reported by Hepburn et al. (13) are given in Table VII. Table VIII summarizes the results in a form that facilitates comparison between experiment and theory. At E_T = 7.0 kcal/mole, the relative ordering of the computed abstraction cross sections on all potential-energy surfaces is in accord with the molecular beam data. The best quantitative agreement with experiment at E_T = 7.0 kcal/mole is obtained with surface I, which has an abstraction barrier of 1.01 kcal/mole. However, a consideration of the error limits for these results suggests

TABLE III

SURFACE I: RELATIVE CROSS SECTIONS

Rxn.	N	E_T	$\sigma_{(abs.)}(a\cdot u)^2$	$\sigma_{exc.}(a\cdot u)^2$	$\sigma^{Rel.}_{Abs.}$
(H,H)	1,000	7.2	1.72 ± 0.38	5.45 ± 0.41	1.00 ± 0.00
(H,D)	1,000	7.2	1.41 ± 0.34	3.2 ± 0.30	0.82 ± 0.27
(D,H)	10,000*	7.0	2.40 ± 0.14	5.43 ± 0.14	1.40 ± 0.32
(D,D)	1,000	7.0	2.04 ± 0.39	4.32 ± 0.36	1.19 ± 0.35
(H,H)	1,000	2.0	1.0 ± 0.3		0.58 ± 0.22
(H,D)	1,000	2.0	0.69 ± 0.21		0.40 ± 0.15
(D,H)	10,000*	2.0	1.4 ± 0.1		0.81 ± 0.19
(D,D)	1,000	2.0	0.72 ± 0.25		0.42 ± 0.17

*In these cases, Important Sampling method was used.

E_T is in kcal/mole.

TABLE IV

SURFACE II: CROSS SECTION RESULTS

Reaction	$\sigma_{abs.}(a\cdot u)^2$	$\sigma^{Rel.}_{abs.}$	$\sigma_{(exc.)}(a\cdot u)^2$
		E_T = 7 kcal/mole	
(H,H)	1.78 ± 0.37	1.00 ± 0.00	5.57 ± 0.42
(H,D)	1.72 ± 0.38	0.97 ± 0.29	3.2 ± 0.30
(D,H)	2.67 ± 0.46	1.50 ± 0.40	6.62 ± 0.47
(D,D)	2.12 ± 0.39	1.19 ± 0.33	5.0 ± 0.4
		E_T = 2 kcal/mole	
(H,H)	1.85 ± 0.42	1.04 ± 0.32	
(H,D)	1.24 ± 0.32	0.70 ± 0.23	
(D,H)	1.82 ± 0.38	1.02 ± 0.30	
(D,D)	1.08 ± 0.32	0.61 ± 0.22	

Number of trajectories: 1,000.

TABLE V

SURFACE III: CROSS SECTION RESULTS

Reaction	$\sigma_{abs.}(a\cdot u)^2$	$\sigma^{Rel.}_{abs.}$	$\sigma_{exc.}(a\cdot u)^2$
		E_T = 7.0 kcal/mole	
(H,H)	1.64 ± 0.37	1.00 ± 0.00	5.26 ± 0.40
(H,D)	1.88 ± 0.39	1.15 ± 0.35	2.74 ± 0.27
(D,H)	2.95 ± 0.51	1.80 ± 0.51	6.00 ± 0.44
(D,D)	2.05 ± 0.39	1.25 ± 0.37	4.37 ± 0.36
		E_T = 2.0 kcal/mole	
(H,H)	2.02 ± 0.44	1.23 ± 0.39	
(H,D)	1.56 ± 0.35	0.95 ± 0.30	
(D,H)	2.43 ± 0.47	1.48 ± 0.44	
(D,D)	1.84 ± 0.42	1.12 ± 0.36	

Number of trajectories: 1,000.

TABLE VI

SURFACE III: IMPORTANT SAMPLING CUMULATIVE CROSS SECTION RESULTS

Reaction	$\sigma_{abs.}(a\cdot u)^2$	$\sigma^{Rel.}_{abs.}$	$\sigma_{exc.}(a\cdot u)^2$
		E_T = 7 kcal/mole	
(H,H)*	2.10 ± 0.13	1.00 ± 0.00	4.54 ± 0.13
(H,D)	1.57 ± 0.15	0.748 ± 0.085	2.72 ± 0.14
(D,H)	2.60 ± 0.22	1.24 ± 0.13	5.5 ± 0.2
(D,D)	2.32 ± 0.18	1.10 ± 0.11	3.88 ± 0.17
(T,T)	2.29 ± 0.18	1.10 ± 0.11	3.64 ± 0.16
		E_T = 2 kcal/mole	
(H,H)	1.88 ± 0.18	0.90 ± 0.10	
(H,D)*	1.59 ± 0.12	0.757 ± 0.074	
(D,H)	2.39 ± 0.19	1.14 ± 0.11	
(D,D)	1.78 ± 0.18	0.8 ± 0.1	
		E_T = 0.5 kcal/mole	
(H,H)	0.72 ± 0.11	0.343 ± 0.057	
(H,D)	0.82 ± 0.12	0.390 ± 0.062	
(D,H)	1.13 ± 0.18	0.538 ± 0.092	
(D,D)	0.68 ± 0.11	0.324 ± 0.056	

*Results are from 10,000 trajectories. Rest of the values are from 5,000 trajectories.

TABLE VII

RELATIVE ABSTRACTION CROSS SECTIONS OBTAINED FROM MOLECULAR BEAM MEASUREMENT[a]

Reaction	Relative Cross Section[b]
	E_T = 7.0 kcal/mole
(H,H)	1.00
(H,D)	0.89 ± 0.06
(D,H)	1.56 ± 0.14
(D,D)	1.46 ± 0.14
	E_T = 2.0 kcal/mole
(H,H)	1.32 ± 0.27
(H,D)	1.09 ± 0.27
(D,H)	1.40 ± 0.27
(D,D)	1.40 ± 0.27

[a]Reference 13.

[b]All values are normalized to the (H,H) result at E_T = 7.0 kcal/mole.

TABLE VIII

COMPARISON OF COMPUTED RELATIVE ABSTRACTION CROSS SECTIONS WITH MOLECULAR BEAM DATA

Reaction	Relative Cross Sections[a]			
	Experiment[b]	Surface I	Surface II	Surface III
	E_T = 7.0 kcal/mole			
(D,H)	1.56 ± 0.14	1.40 ± 0.32	1.50 ± 0.40	1.24 ± 0.13
(D,D)	1.46 ± 0.14	1.19 ± 0.35	1.19 ± 0.33	1.10 ± 0.11
(H,H)	1.00	1.00	1.00	1.00
(H,D)	0.89 ± 0.06	0.82 ± 0.27	0.97 ± 0.29	0.75 ± 0.08
	E_T = 2.0 kcal/mole			
(D,H)	1.40 ± 0.27	0.81 ± 0.19	1.02 ± 0.30	1.14 ± 0.11
(D,D)	1.40 ± 0.27	0.42 ± 0.17	0.61 ± 0.22	0.80 ± 0.10
(H,H)	1.32 ± 0.27	0.58 ± 0.28	1.04 ± 0.32	0.90 ± 0.10
(H,D)	1.09 ± 0.27	0.40 ± 0.15	0.70 ± 0.23	0.76 ± 0.07

[a]All values are normalized to the (H,H) result at E_T = 7.0 kcal/mole.

[b]Reference 13.

that this agreement is fortuitous.

The results for surface I at E_T = 2.0 kcal/mole clearly show that the abstraction barrier is too large on this surface. The computed cross sections decrease to one-half to one-third of the measured values, and the qualitative ordering for (D,D) and (H,H) cross sections is inverted, although this is likely a statistical problem. At this energy, the best results are obtained on surface III, which has an abstraction barrier of 0.19 kcal/mole. For this surface, the relative cross sections are in much better agreement with experiment, and the qualitative ordering is essentially correct. When the magnitude of the experimental error is taken into account, the agreement is seen to be good. We therefore conclude that of the surfaces studied the topographical features of surface III most nearly reproduce those of the actual (H_2Br) surface.

The computed variation of the relative abstraction cross sections with relative translational energy for surface III is shown in Figure 9. It should be noted that the relative ordering and slopes of the curves in the low-energy range suggest that the (H,D) cross section will become the largest of the four results as $E_T \rightarrow 0$.

The "cone of acceptance" model described by Hepburn and coworkers (13) correctly predicts the order of reactivity of (D,H) and (H,D) at E_T = 7.0 kcal/mole, i.e., (D,H) > (H,D). According to this model, (H,H) and (D,D) should be of equal reactivity. However, in this work (D,D) is found to be more reactive than (H,H), as also found by Hepburn and coworkers (13). Nevertheless, the computed relative abstraction cross sections for (H,H), (D,D) and (T,T) are very nearly the same as well. Consequently, the present calculations support the essential

Figure 9. Relative Abstraction Cross Sections on Surface III as a Function of Relative Translational Energy.

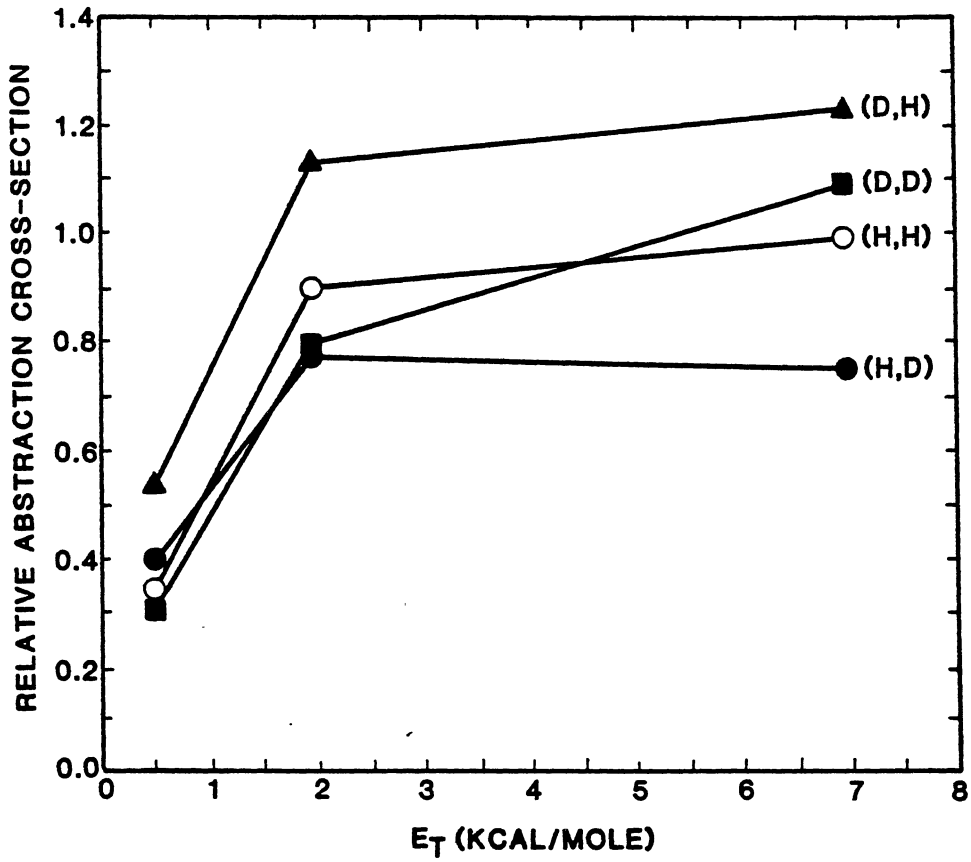
RELATIVE ABSTRACTION CROSS-SECTION
1.4
1.2
1.0
0.8
0.6
0.4
0.2
0.0
0
1
2
3
4
5
6
7
8
E_T (KCAL/MOLE)
(D,H)
(D,D)
(H,H)
(H,D)

concept suggested by the "cone of acceptance" model.

The relative cross section ordering for the exchange reaction is

$$(D,H) > (H,H) > (D,D) > (T,T) > (H,D).$$

These results may be qualitatively explained by combining the Hepburn and coworkers' (13) "cone of acceptance" model with zero-point energy considerations. That is, we have (D,H) > (H,D) because of the significantly greater cone of acceptance present in the (D,H) reaction. The "cone of acceptance" argument would suggest that

$$(H,H) = (D,D) = (T,T),$$

however, the zero-point energy of the reactant diatomic molecule increases in the order $(ZPE)_{HBr} > (ZPE)_{DBr} > (ZPE)_{TBr}$. Since the zero-point energy should assist the exchange reaction, the observed cross section ordering is not unexpected.

The product energy distributions have been computed for all reactions studied. Figures 10 through 19 show results typical of those obtained for each of the 36 possible combinations at E_T = 7.0 or 2.0 kcal/mole. The average fractions of the total available energy partitioned into vib-rotation of the product molecule for each case computed are listed in Table IX. These results clearly show that the first moment of the energy partitioning is insensitive to the small variations in surface topography present in Surfaces I, II and III. However, if more significant alterations of the potential surface are made, the energy partitioning will be affected. This point is demonstrated by the fact that White and coworkers (16a) obtained $\langle f_E \rangle = 0.60$ on a potential surface whose topography is significantly different than those employed in the present study. The average energy partitioning is also almost independent of initial relative translational energy.

Figure 10. Product Energy Distribution for (H,H) Exchange Reaction on Surface I at E_T = 7.0 kcal/mole.

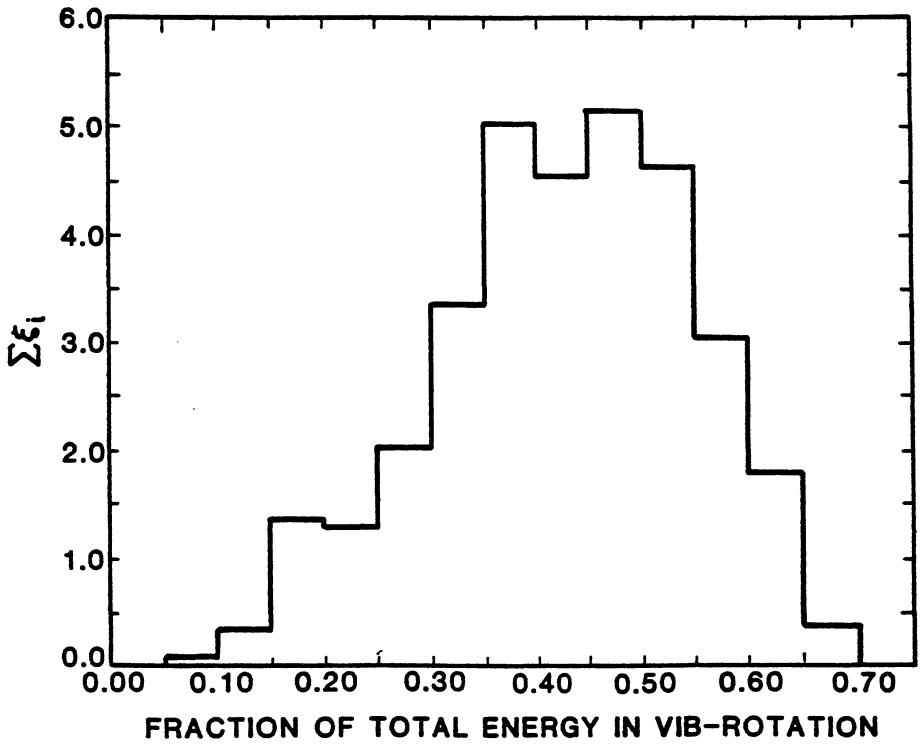
6.0
5.0
4.0
3.0
2.0
1.0
0.0
$\Sigma\xi_i$
0.00
0.10
0.20
0.30
0.40
0.50
0.60
0.70
FRACTION OF TOTAL ENERGY IN VIB-ROTATION

Figure 11. Product Energy Distribution for (D,H) Exchange Reaction on Surface I at E_T = 7.0 kcal/mole.

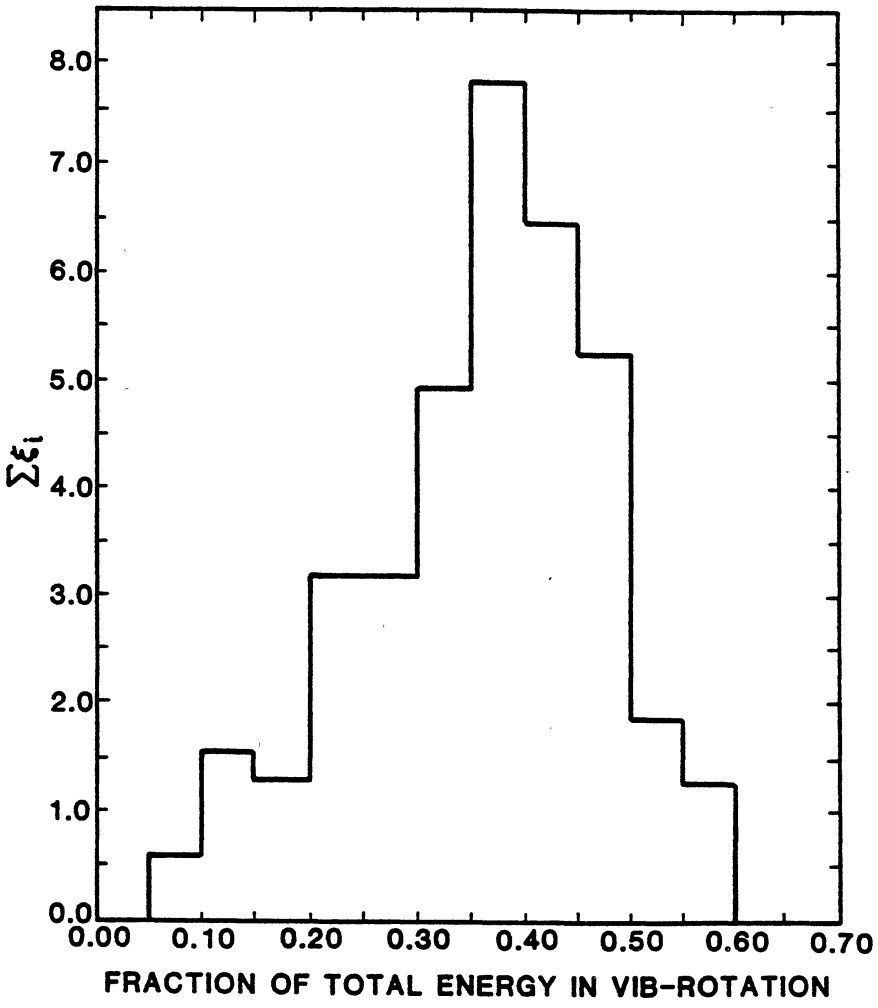
8.0
7.0
6.0
5.0
4.0
3.0
2.0
1.0
0.0
$\Sigma\xi_i$
0.00
0.10
0.20
0.30
0.40
0.50
0.60
0.70
FRACTION OF TOTAL ENERGY IN VIB-ROTATION

Figure 12. Product Energy Distribution for (H,H) Abstraction Reaction on Surface III at E_T = 0.5 kcal/mole.

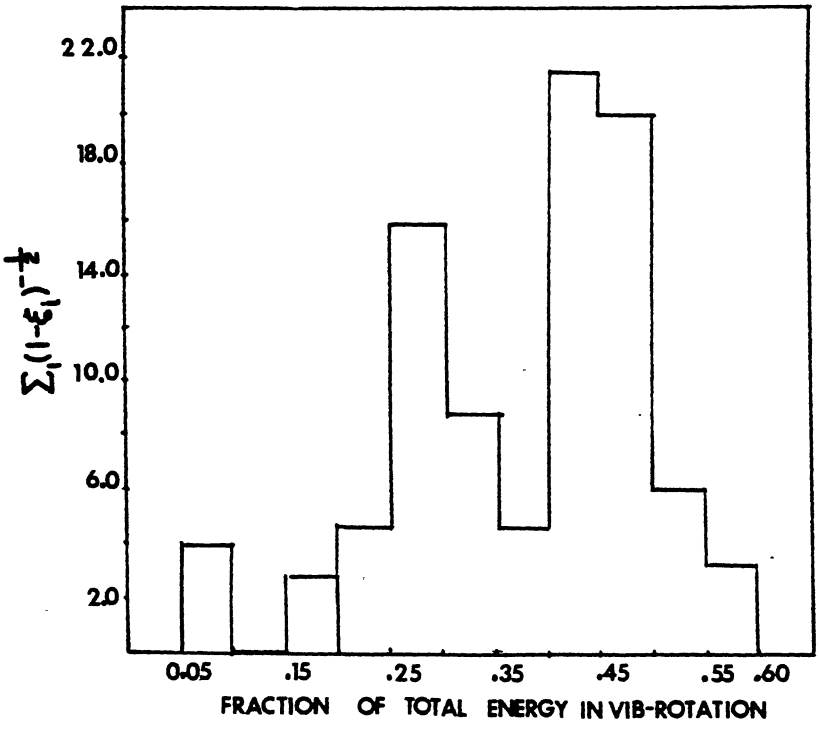
22.0
18.0
14.0
10.0
6.0
2.0
0.05
.15
.25
.35
.45
.55
.60
FRACTION OF TOTAL ENERGY IN VIB-ROTATION

Figure 13. Product Energy Distribution for (H,D) Abstraction Reaction on Surface III at E_T = 0.5 kcal/mole.

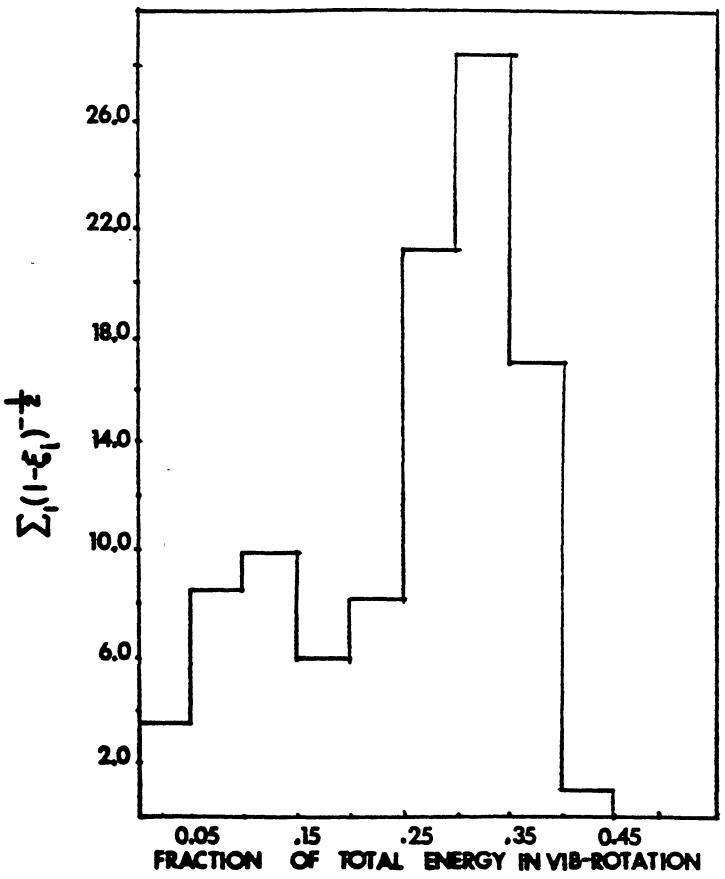
26.0
22.0
18.0
14.0
10.0
6.0
2.0
0.05
.15
.25
.35
0.45
FRACTION OF TOTAL ENERGY IN VIB-ROTATION
$\Sigma^+ (^1\Sigma - ^1\Sigma)$

Figure 14. Product Energy Distribution for (H,D) Abstraction Reaction on Surface III at E_T = 2.0 kcal/mole.

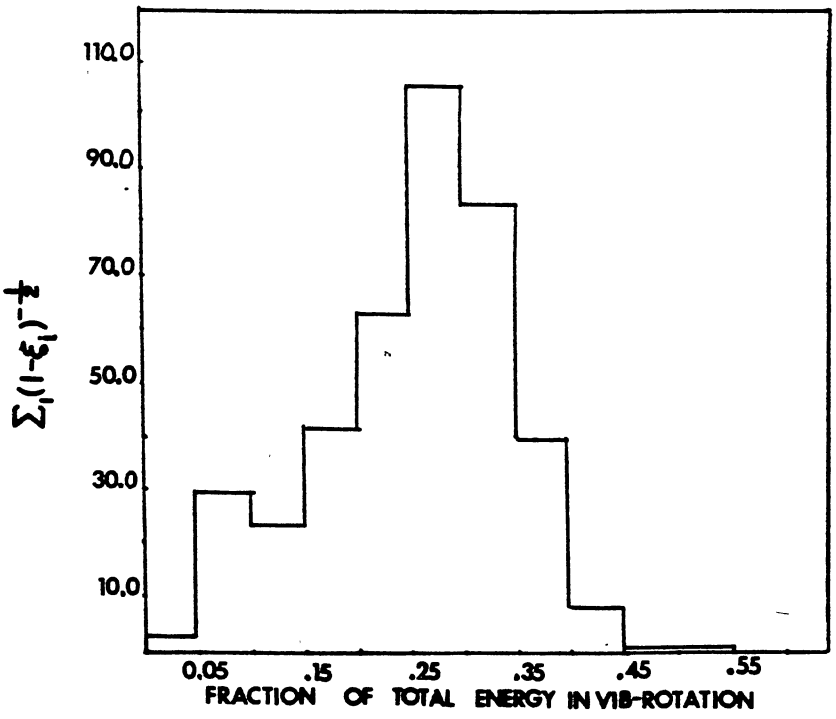
110.0
90.0
70.0
50.0
30.0
10.0
$\sum_i (1-\xi_i)^{-\frac{1}{2}}$
0.05
.15
.25
.35
.45
.55
FRACTION OF TOTAL ENERGY IN VIB-ROTATION

Figure 15. Product Energy Distribution for (D,H) Abstraction Reaction on Surface I at E_T = 7.0 kcal/mole.

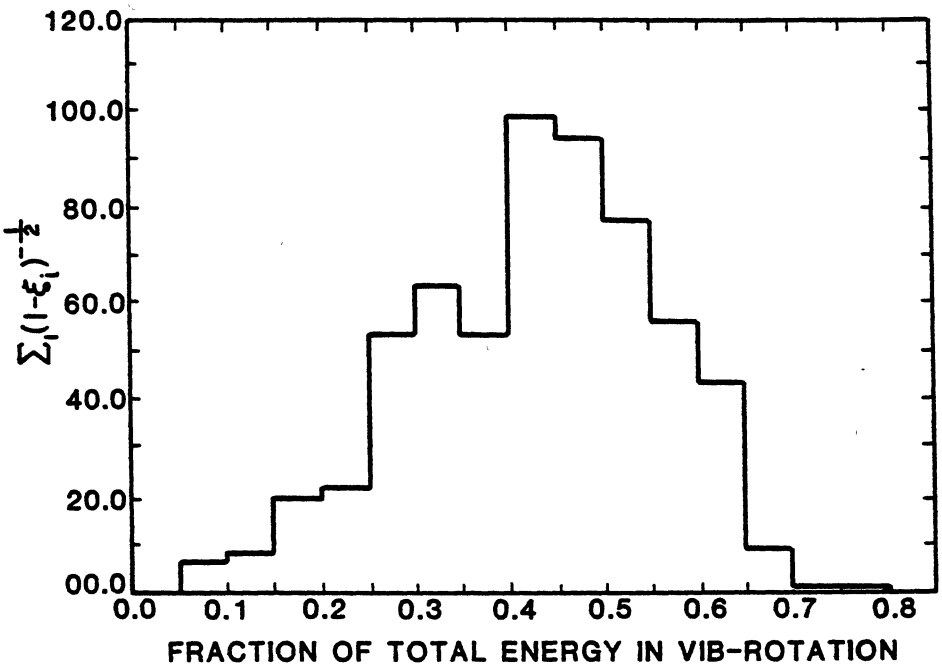
120.0
100.0
80.0
60.0
40.0
20.0
00.0
$\sum_i (1-\xi_i)^{-\frac{1}{2}}$
0.0
0.1
0.2
0.3
0.4
0.5
0.6
0.7
0.8
FRACTION OF TOTAL ENERGY IN VIB-ROTATION

Figure 16. Differential Scattering Cross Section for Br Scattering in (D,H) Abstraction Reaction on Surface I at E_T = 2.0 kcal/mole.

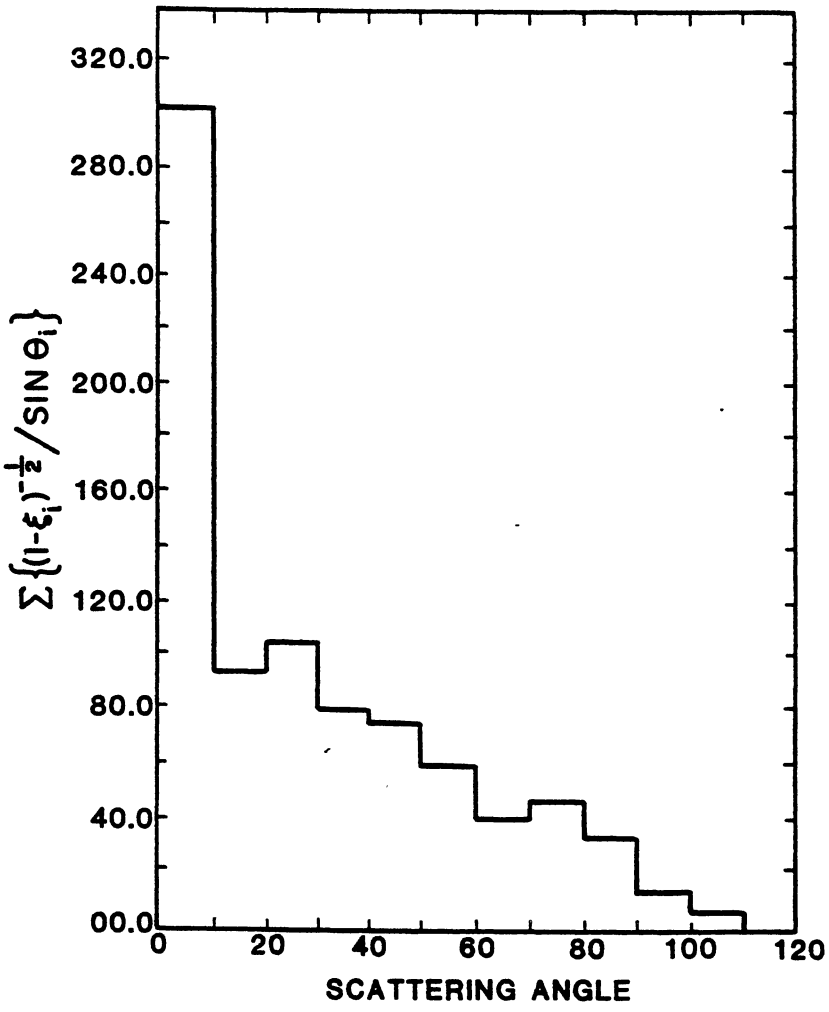
320.0
280.0
240.0
200.0
160.0
120.0
80.0
40.0
00.0
0
20
40
60
80
100
120
SCATTERING ANGLE
$\Sigma\{(1-\xi_i)^{-\frac{1}{2}}/\sin\theta_i\}$

Figure 17. Differential Scattering Cross Section for Br Scattering in (H,H) Abstraction Reaction on Surface III at E_T = 0.5 kcal/mole.

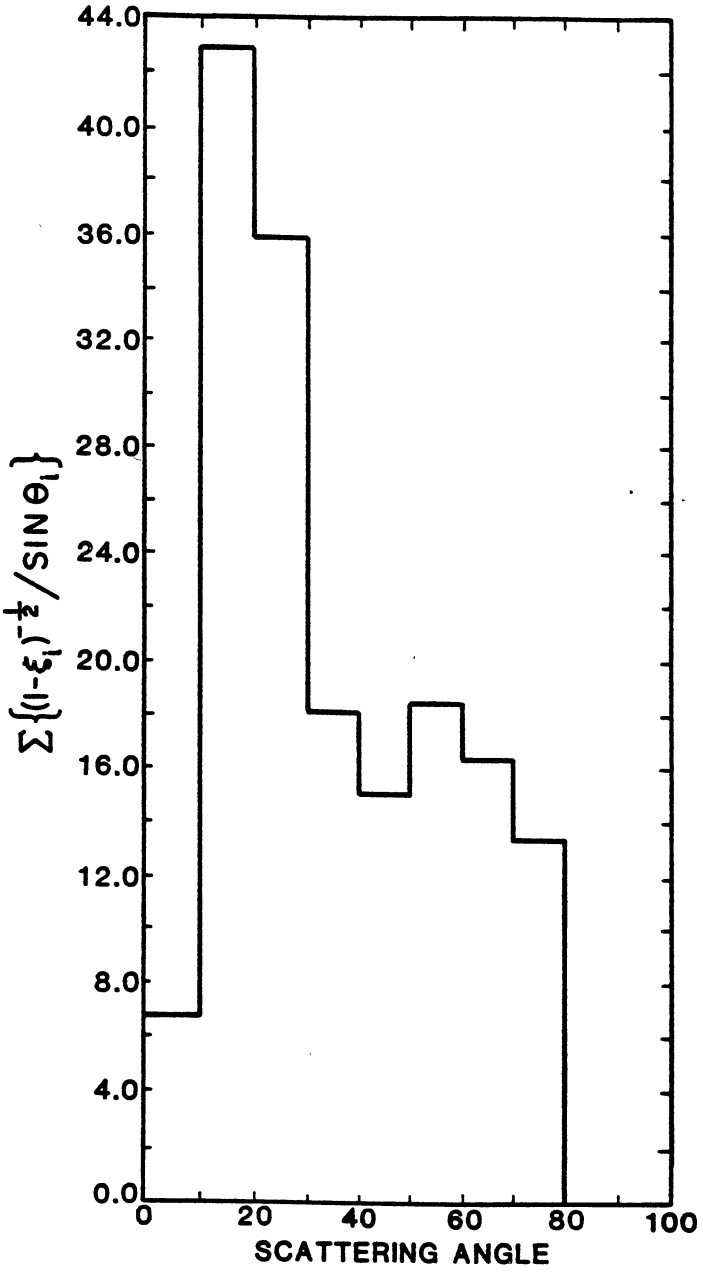
44.0
40.0
36.0
32.0
28.0
24.0
20.0
16.0
12.0
8.0
4.0
0.0
0
20
40
60
80
100
SCATTERING ANGLE
$\Sigma\{(1-\xi_i)^{-\frac{1}{2}}/\sin\theta_i\}$

Figure 18. Differential Scattering Cross Section for H Atom Scattering in (D,H) Exchange Reactions on Surface III at E_T = 7.0 kcal/mole.

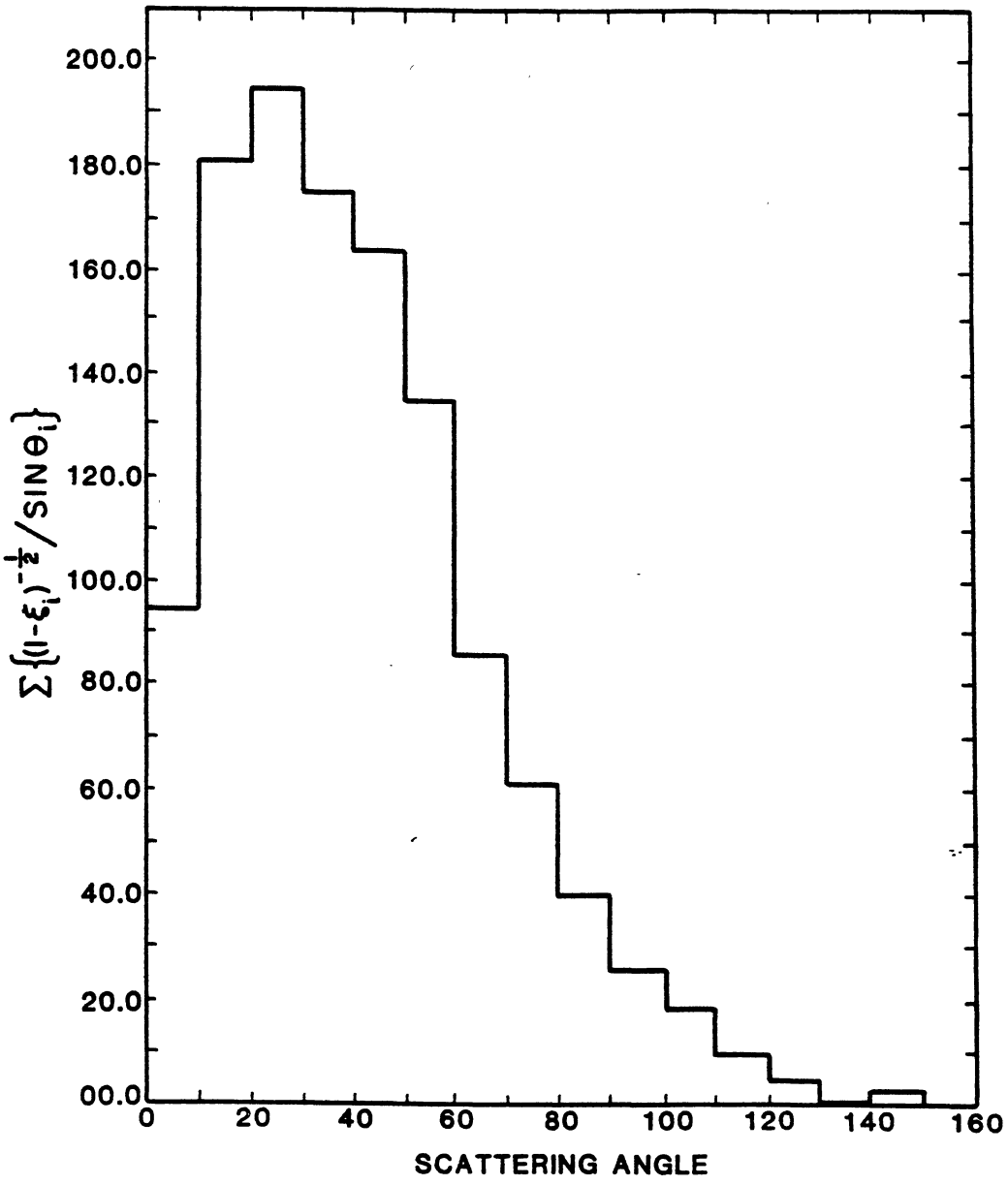
200.0
180.0
160.0
140.0
120.0
100.0
80.0
60.0
40.0
20.0
00.0
0
20
40
60
80
100
120
140
160
SCATTERING ANGLE
$\Sigma\{(1-\epsilon_i)^{-\frac{1}{2}}/\sin\theta_i\}$

Figure 19. Differential Scattering Cross Section for H Atom Scattering in (H,H) Exchange Reaction on Surface III at E_T = 7.0 kcal/mole.

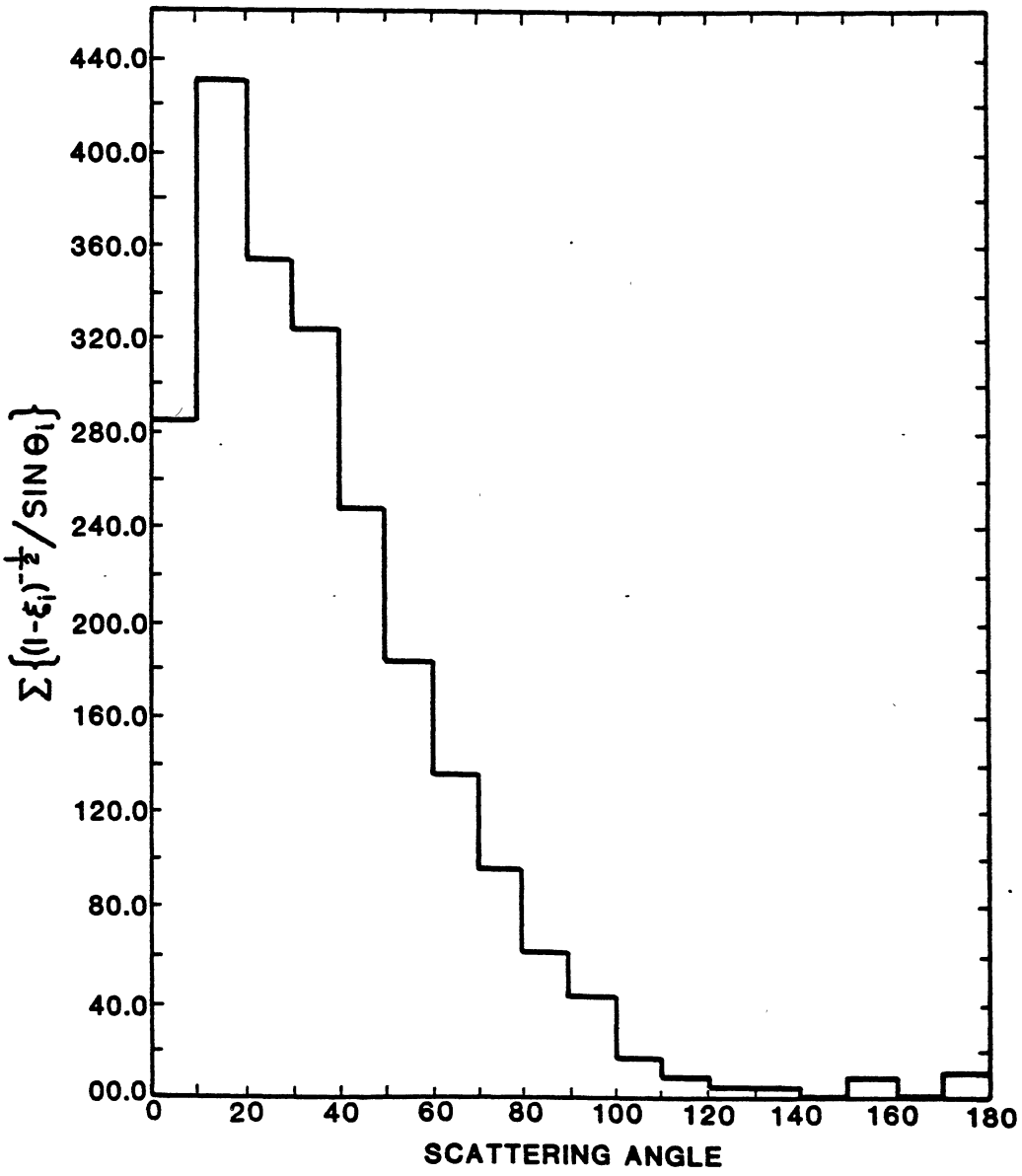
440.0
400.0
360.0
320.0
280.0
240.0
200.0
160.0
120.0
80.0
40.0
00.0
0
20
40
60
80
100
120
140
160
180
SCATTERING ANGLE
$\Sigma\{(1-\xi_i)^{-\frac{1}{2}}/\sin\theta_i\}$

TABLE IX

AVERAGE ENERGY PARTITIONING ON SURFACES I, II AND III FOR ABSTRACTION AND EXCHANGE REACTIONS

Reaction	E_T (kcal/mole)	$\langle f_E \rangle$[a]		
		Surface I	Surface II	Surface III
		Abstraction		
(H,D)	7	0.25	0.25	0.24
(H,D)	2	0.29	0.25	0.25
(D,H)	7	0.43	0.44	0.43
(D,H)	2	0.50	0.51	0.48
(D,D)	7	0.27	0.25	0.30
(D,D)	2	0.35	0.35	0.32
(H,H)	7	0.34	0.32	0.33
(H,H)	2	0.41	0.41	0.34
		Exchange		
(H,D)	7	0.41	0.43	0.42
(D,H)	7	0.37	0.37	0.38
(D,D)	7	0.38	0.39	0.38
(H,H)	7	0.42	0.44	0.43

[a]Average fraction of the total energy partitioned into the vib-rotation of the product molecule.

Consequently, energy partitioning measurements are unlikely to provide useful data with regard to elucidation of the fine details of the potential-energy surface. The only obvious variation of the data given in Table IX is the average $\langle f_E \rangle$ for the (D,H) abstraction reaction which is significantly greater than the corresponding values for the other abstraction reactions.

Computed differential cross sections for both abstraction and exchange reactions show that all reactions occur through a rebound mechanism with the atomic product being scattered forward, i.e., in the direction of the initial relative velocity vector. The relatively small absolute cross sections for these reactions suggest that this should be the principal mode of reaction. Typical differential scattering distributions are shown in Figures 16 through 19.

The thermal rates for the abstraction reactions have been measured at 300 K by Steiner (27), Endo and Glass (8), and by Husain and Slater (9). Their results are given in Table X. We have computed the thermal abstraction rates for (H,D) and (D,H) at 300 K from the results of 20,000 trajectories on surface III using importance sampling for the impact parameter. These results are also given in Table X.

As can be seen, the more recent rate coefficient data reported by Husain and Slater (9) generally exceed the corresponding values reported by Endo and Glass (8) by about a factor of two or three. The theoretical results are about a factor of 2 larger than the Husain-Slater data and correspondingly larger than the values obtained by Endo and Glass. In general, the degree of accord between theory and experiment obtained here is significantly greater than reported by White (16b) and by Truhlar and Kuppermann (28) who obtained absolute rates too large by

TABLE X

RATE COEFFICIENT AND ISOTOPE EFFECTS FOR THE ABSTRACTION REACTIONS AT 300 K

Reaction	$k \times 10^{12}$ (cm^3/molecule-sec)			
	Endo & Glass[a]	Husain & Slater[b]	Steiner[c]	Theory[d]
(H.H)	3.71 ± 0.14	6.0 ± 0.1	2.81	
(H,D)	2.69 ± 0.13	4.7 ± 0.1	-	10.53
(D,H)	1.69 ± 0.13	4.1 ± 0.1	-	7.65
(D,D)	1.24 ± 0.15	2.7 ± 0.1	-	
	Isotope Effects			
(H,D)/(D,H)	1.59	1.15	-	1.38

[a]Reference 8.

[b]Reference 9.

[c]Reference 27.

[d]Present calculation on Surface III.

factors of 10 and 100, respectively, using different potential surface formulations.

The computed (H,D)/(D,H) isotope effect falls between the two experimental values given in Table X. It is interesting to note that while the abstraction reaction cross section for (D,H) exceeds that for (H,D) for $E_T \geq 0.5$ kcal/mole, the rate coefficients are reversed in magnitude. This is due to two factors. First, the rate coefficient is proportional to the collision frequency whereas the cross section is not. This introduces a factor of $\sqrt{2}$ in favor of the (H,D) abstraction due to the smaller (H,D) reduced mass. Secondly, the (H,D) cross section may invert with the (D,H) cross section at low collision energy (see Figure 9). At 300 K, the cross sections in the lower energy range will be the most heavily weighted.

An estimate of the thermal activation energy for the abstraction reaction has been obtained by computation of the (H,D) and (D,H) rate coefficients at 250 K from the results of 20,000 trajectories on surface III. The result is $E_a = 835$ cal/mole. Steiner (27) reported a value of 900 cal/mole and Endo and Glass (8) obtained 2100 ± 500 cal/mole.

CHAPTER IV

CONCLUSIONS

Reaction cross sections, product energy partitioning distributions, differential scattering cross sections, thermal rate coefficients, isotope effect ratios and thermal activation energies for the reactions

$$M + M'Br \begin{cases} \nearrow MM' + Br & \text{abstraction} \\ \searrow MBr + M' & \text{exchange} \end{cases}$$

with (M,M' = H or D) have been computed on three different LEPS potential-energy surfaces from the results of 139,000 quasiclassical trajectories. The surfaces all have identical product and reactant valleys and exchange reaction barriers between 4.83 to 5.20 kcal/mole with no attractive hollows with a depth greater than 0.2224 kcal/mole. The abstraction barrier on the surfaces varied from 0.18 to 1.01 kcal/mole. Thus, each surface possesses all of the topographical features suggested by recent molecular beam experiments (13, 14).

The relative abstraction cross sections were found to decrease much more rapidly with relative collision energy than is indicated by the molecular beam experiments (13, 14) if the abstraction barrier was greater than 0.65 kcal/mole. The best agreement with experiment was obtained with an abstraction barrier of 0.19 kcal/mole. For this surface, the relative ordering of abstraction cross sections for the various isotopic combinations was found to be in accord with the

data reported by Hepburn and coworkers (13). Qualitatively, the computed abstraction cross sections are in accord with the "cone of acceptance" model previously described by Hepburn and coworkers (13).

Thermal rate coefficients at 300 K computed on surface III (abstraction barrier of 0.19 kcal/mole) are about a factor of 2 larger than recently reported measurements of Husain and Slater (9) and are a factor of 4 larger than the results obtained by Endo and Glass (8). The extent of agreement between theory and experiment is generally much greater than that previously obtained using different potential-energy surfaces (16b, 28). Computed thermal isotope ratios fall between the two measured results (8, 9).

Computed product energy distributions have been obtained for all isotopic combinations of the abstraction and exchange reactions. In general, these distributions are nearly independent of both the topography of the potential-energy surface and the relative collision energy. The average fraction of the available energy partitioned into product relative translational motion is about 0.40, which is significantly less than the result previously reported by White and coworkers (16b).

Differential scattering cross sections for all isotopic combinations of both the exchange and the abstraction reactions are peaked between 0 and 10^{o} for the atomic product scattering. (Small angles correspond to scattering in the direction of the initial relative velocity vector.) Consequently, these reactions take place by a molecular rebound mechanism. Similar results have previously been reported by Parr and Kuppermann (15) and by White and coworkers (16).

BIBLIOGRAPHY

(1) a) Raff, L. M., Stivers, L., Porter, R. N., Thompson, D. L. and Sims, L. B., J. Chem. Phys. 52, 3449 (1970);

b) Porter, R. N., Sims, L. B., Thompson, D. L. and Raff, L. M., J. Chem. Phys. 58, 2855;

c) Parr, C. A. and Truhlar, D. G., J. Phys. Chem. 75, 1844 (1971);

d) Ellison, F. O. and Patel, J. C., J. Am. Chem. Soc. 86, 2115 (1964).

(2) Truhler, D. G. and Kuppermann, A., J. Phys. Chem. 73, 1722 (1969).

(3) Levine, R. D. and Bernstein, R. B., Chem. Phys. Lett. 29, 1 (1974).

(4) McDonald, J. D. and Herschback, D. R., J. Chem. Phys. 62, 4740 (1975).

(5) Beck, W. H., Gotting, R., Toennies, J. P. and Winkelmann, K., J. Chem. Phys. 72, 2896 (1980).

(6) Bauer, W., Rusin, L. Y. and Toennies, J. P., J. Chem. Phys. 68, 4490 (1978).

(7) Persky, A. and Kuppermann, A., J. Chem. Phys. 61, 5035 (1974).

(8) Endo, H. and Glass, G. P., J. Phys. Chem. 80, 1519 (1976).

(9) Husain, D. and Slater, N. K. H., J. Chem. Soc. Faraday Trans. 2 76, 276 (1980).

(10) Botschwina, P. and Meyer, W., J. Chem. Phys. 67, 2390 (1977).

(11) Parr, C. A. and Truhlar, D. G., J. Phys. Chem. 75, 1844 (1971).

(12) Dunning, T. H., Jr., J. Phys. Chem. 88, 2469 (1984).

(13) Hepburn, J. W., Klimek, D., Liu, K., Macdonald, R. G., Northrup, F. J. and Polanyi, J. C., J. Chem. Phys. 74, 6226 (1981).

(14) a) Bauer, W., Rusin, L. Y., Toennies, J. P., and Walsachewski, K., J. Chem. Phys. 66, 3837 (1977);

b) Schwalim, U. and Toennies, J. P., Chem. Phys. Lett. 63, 17 (1978);

(15) Parr, C. A., Ph.D. Thesis, California Institute of Technology, 1969.

(16) a) Pace, S. A. and White, J. M., Int. J. Chem. Kinet. 7, 951 (1975);

b) White, J. M., J. Chem. Phys. 65, 3674 (1976);

c) Ibid, p. 4482.

(17) Kuntz, P. J., Nemeth, E. M., Polanyi, J. C., Rosner, S. D. and Young, C. E., J. Chem. Phys. 44, 1168 (1966).

(18) Kellerhals, G. E., Sathyamurthy, N. and Raff, L. M., J. Chem. Phys. 64, 818 (1976).

(19) Porter, R. N., Sims, L. B., Thompson, D. L. and Raff, L. M., J. Chem. Phys. 58, 2855 (1973).

(20) Raff, L. M., Thompson, D. L., Sims, L. B. and Porter, R. N., J. Chem. Phys. 56, 5998 (1972).

(21) Protter, M. H. and Morrey, C. B., Jr., in College Calculus with Analytic Geometry (Addison Wesley Publishing Company, London), Second Edition, 1970, p. 750.

(22) Porter, R. N. and Raff, L. M., Classical Trajectory Methods in Molecular Collisions, in Modern Theoretical Chemistry, ed. Miller, W. H. (Plenum Press, New York, 1976) p. 1.

(23) Raff, L. M. and Thompson, D. L., The Classical Trajectory Approach to Reactive Scattering in The Theory of Chemical Reaction Dynamics, Ed. Baer, M. (CRC Press, Boca Raton, Fl, 1985).

(24) Truhlar, D. G. and Muckermann, J. T., "Atom-molecule Collision Theory: A Guide for the Experimentalist", Ed. Bernstein, R. B. (Plenum Press, New York, 1979), p. 505.

(25) Faist, M. B., Muckerman, J. T. and Schubert, F. E., J. Chem. Phys. 69, 4087 (1978).

(26) Karplus, M., Porter, R. N. and Sharma, R. D., J. Chem. Phys. 43, 3259 (1965).

(27) Steiner, W., Proc. R. Soc. A, 173, 531 (1939).

(28) Truhlar, D. G. and Kuppermann, A., J. Phys. Chem. 73, 1722 (1969).

VITA

Meenakshisundaram Padmasani Sudhakaran

Candidate for the Degree of

Master of Sceince

Thesis: THEORETICAL INVESTIGATIONS OF H(D) + HBr(DBr) ABSTRACTION AND EXCHANGE REACTIONS

Major Field: Chemistry

Biographical:

Personal Data: Born in India, on July 27, 1959.

Education: Graduated from M. C. N. High School in 1975; received the Bachelor of Science degree in Chemistry from the University of Madras, India, in 1979; received the Master of Science degree in Chemistry from the University of Madras, India, in 1981; completed requirements for the Master of Science degree at Oklahoma State University in May, 1985.

Professional Experience: From June 8, 1981 to September 11, 1981 worked as a Research Assistant in Chemistry in the Yeddanapalli Institute of Educational Research, Loyola College, Madras, India, under the guidance of Dr. N. S. Gnanapragasam, Ph.D. in preparing a revised version of the General Chemistry Lecture Notes and Lab Manual of this above mentioned college. Presently working as a Graduate Teaching Assistant at OSU.

Professional Organizations: Member of Phi Lambda Upsilon, Honorary Chemical Society.